Pattern structures on generalized nonlinear Schrödinger equations with various nonlinear terms

Cangtao Zhou,[1,2] X. T. He,[1,2] and Tianxing Cai[2]
[1] *China Center of Advanced Science and Technology (World Laboratory), P.O. Box 8730, Beijing 100080, China*
[2] *Laboratory of Computational Physics and Center for Nonlinear Studies, Institute of Applied Physics and Computational Mathematics, P.O. Box 8009, Beijing 100088, China**
(Received 7 June 1994)

The spatiotemporal characteristics on a series of the generalized nonlinear Schrödinger equations (NSE's) in one- and two-dimensional space have been systematically discussed. The current investigations show that the high order Hamiltonian perturbation can lead to the destruction of the coherent structures and the formation of the spatiotemporally complicated patterns. The route from the coherent patterns to the complicated ones experiences a quasiperiodic route. For two-dimensional problems, the numerical experiments illustrate that the singular solution, spatiotemporal chaos, and pseudorecurrence can appear in the same NSE with the increase of the saturable nonlinear effects, where the spatial patterns and the energy partition of the system in the Fourier modes exhibit completely different dynamic behaviors. In particular, the symmetric destruction of the spatial patterns is associated with the energy in the nondiagonal modes.

PACS number(s): 52.35.Mw, 47.10.+g, 05.45.+b, 52.40.Db

I. INTRODUCTION

The generalized nonlinear Schrödinger equation (NSE)

$$iE_t + \nabla^2 E + F(|E|^2)E = 0, \tag{1.1}$$

in which the potential F is a differential smooth real function, is one of the basic evolution models for nonlinear waves in various branches of a wave train in conservative, disperse systems. Early applications of the NSE were in the context of nonlinear optics where it described the propagation of light beams in nonlinear media [1]. Also, it has been applied to gravity waves on deep water, for which the predicted modulational instability and envelope soliton formation have been clearly demonstrated experimentally [2]. In plasma physics, it was first derived for nonlinear hydromagnetic waves by Taniuti and Washimi using the reductive perturbation method [3].

For the one-dimensionally cubic NSE, the Lax pair has been found by Zakharov and Shabat and the inverse scattering transform (IST) is well established [4]. The infinite integrals of motion and N-soliton solutions, which are associated with integrability, can also be obtained by IST [5]. For the case of high-dimensional space, Rasmussen and Rypdal [6] showed that focusing singularities can occur in two- and three-dimensional space, and gave the condition for the singular solution analytically.

For Eq. (1.1), the Lagrangian density is

$$L = \frac{i}{2}(E^* E_t - E E_t^*) - |\nabla E|^2 + f(|E|^2), \tag{1.2}$$

where $f(|E|^2) = \int_0^{|E|^2} F(s)ds$. According to the Norther theorem, we can obtain the following invariants: the quasiparticle number

$$N = \int |E|^2 d\mathbf{X}, \tag{1.3}$$

the momentum

$$P = \frac{i}{2}\int (E_{\mathbf{X}} E^* - E E_{\mathbf{X}}^*) d\mathbf{X}, \tag{1.4}$$

the energy

$$H = \int [|E_{\mathbf{X}}|^2 - f(|E|^2)] d\mathbf{X}, \tag{1.5}$$

and the other invariants, for example, angular momentum in the three-dimensional space and the moment of inertia, etc. [6].

Taking the different physical backgrounds into account, some particular types of $F(|E|^2)$ in Eq. (1.1) have frequently been applied. For example [7–28],

$$\text{(i) } F(|E|^2) = |E|^{2q}, \tag{1.6}$$

$$\text{(ii) } F(|E|^2) = |E|^2 - g|E|^4, \tag{1.7}$$

$$\text{(iii) } F(|E|^2) = \frac{|E|^2}{1 + g|E|^2}, \tag{1.8}$$

$$\text{(iv) } F(|E|^2) = \frac{1}{2g}(1 - e^{-2g|E|^2}). \tag{1.9}$$

For model (1.6), a collapse of the nonlinear wave [7,8], when the spatial dimension (D) and the coefficient q sat-

*Mailing address.

isfy $qD \geq 2$, can occur. In nonlinear plasmas, this important process solves the problem of small-K condensation in weak turbulent theory. When $q = 1$, the one-dimensional cubic NSE possesses integrability. Solitons developed by modulational instabilities keep their spatially coherent structures and temporally periodic evolutions. In particular, the well-known Fermi-Pasta-Ulam (FPU) recurrence in connection with deep water waves has been verified experimentally by Lake, Rungaldier, and Ferguson [9] and Yuen *et al.* [10]. The simple and complex recurrence phenomena were discussed numerically by Yuen and Ferguson [11] and analytically by Stiassnie and Kroszynski [12].

For model (1.7), the fifth order correction to the cubic term arises from the nonlinear interaction between Langmuir waves and electrons [13]. The coupling nonlinear equations, known as Zakharov equations, describe the nonlinear interaction between the high frequency Langmuir wave and the ion-acoustic wave by ponderomotive force. However, a beat frequency interaction between the large amplitude parts of high frequency fields and particles can occur in the nonlinear strong turbulence stages. Under the static approximation, He [13] has obtained a NSE where the potential $F(|E|^2)$ can be expressed by Eq. (1.7) in terms of Vlasov-Maxwell equations. In many-nucleon systems, usually, collision processes of heavy ions are described on classical or quasiclassical levels [14]; it was shown that in the quasiclassical limit the nuclear hydrodynamics equations with the Skyrme forces can be reduced to the nonrelativistic cubic-quintic model for the corresponding choice of variable [15]. For this model, on the other hand, some theoretical work has been obtained analytically and numerically. Puskharov *et al.* [15] obtained solitary wave solutions. Cowan *et al.* [16] numerically showed that these are not solitons, but behave like quasisolitons. Gagnon and Winternitz *et al.* [17,18] presented a large set of exactly analytical traveling wave solutions. Zhou *et al.* [19] also showed that a special periodic solution can be reduced to a solitary wave when the pseudoenergy is zero. The effects of the quintic nonlinear term enhance the amplitude and width of the solitary wave as compared with those for the cubic Langmuir soliton. Cloot *et al.* [20] qualitatively proved the existence of bound solutions by making use of the invariants (1.3) and (1.5). Their numerical results displayed recurrence of solutions. In high space dimensions, the Lie symmetry group was analyzed by Gagnon and Winternitz [21]. They obtained a class of group-invariant solutions.

For model (1.8), Akhmediek *et al.* [22] studied the pseudorecurrence in two-dimensional instability. They showed that an approximated recurrence to an initial homogeneous field can appear, and this pseudorecurrence arises only for a restricted range of the spatially modulational frequency. Mclaughin *et al.* [23] gave the condition for the singular solution.

Model (1.9) is considered as a useful model in homogeneous unmagnetized plasmas [24] and laser-produced plasmas [25–28]. When the phase velocity of the slow plasma oscillation is much smaller than the ion thermal velocity, one can obtain the adiabatic (quasistatic) electron density under the quasineutral approximation: $n_e = n_0 e^{-|E|^2}$. Combining the coupling equation which exhibits the slowly varying complex amplitude $E(\mathbf{X}, t)$ interacting with the low-frequency plasma motion, one can easily obtain Eq. (1.1) involving nonlinear terms (1.9) [24]. In laser plasmas, the light beam filamentation for this model due to the ponderomotive force was extensively studied. Max [25] showed that the self-focusing solution becomes a periodic oscillatory phenomenon, rather than a catastrophic process due to the exponential nonlinearity. Lam *et al.* [26] illustrated that the self-trapped beams are stable. Kaw *et al.* [27] showed that an electromagnetic wave interacting with a plasma is subject to instabilities leading to filamentation. In previous work [28], we showed that the stochastic propagation of beams can accompany the production of the oscillating filamentation instability.

We note that, while previous theoretical and numerical work [7–28] for discussing models (1.6)–(1.9) has concentrated on the solitary wave solutions, the singular solutions, and pseudorecurrence, the problem of the spatiotemporal patterns in one- and high-dimensional space appears to have received very little attention. The main purpose of this paper is to discuss the following questions. Can we choose an available method that completely describes the dynamic behaviors of the spatiotemporal patterns in one- and high-dimensional space? What are the characteristics and patterns of evolution? What is the mechanism for the formation of patterns? These problems are very interesting and important in physics and mathematics. In Sec. II, we constitute the phase space and the initial condition by considering linear analyses. In Sec. III, we describe the integrability and the pattern structures for the one-dimensionally cubic NSE. The spatiotemporal chaos and pattern dynamics in one-dimensional space and two-dimensional space are discussed in Sec. IV and Sec. V, respectively. Some conclusions are summarized in the final section.

II. CHOICE OF INITIAL CONDITION AND CONSTITUTION OF PHASE SPACE

A. Linearized analyses

For the continuum Hamiltonian system (1.1), the dynamic description is dependent on the choice of the initial condition. In particular, we cannot give a reasonable explanation if we take an arbitrary initial condition. Therefore, it is necessary that we choose an available initial condition and constitute a reasonable phase space in order to discuss the spatiotemporally evolutive phenomena of this system. For simplicity, in this work, we only deal with the developing behavior of an initial homogeneous state due to the modulational instability. We assume a homogeneous solution for Eq. (1.1) as $E_s(t) = E_0 e^{i\omega_s t}$, where E_0 satisfies

$$E_0[1 - F(|E_0|^2)] = 0. \tag{2.1}$$

Simultaneously, we define

$$E(\mathbf{X},t) = E_s(t) + \delta E(\mathbf{X},t), \tag{2.2}$$

and linearize Eq. (1.1), and yield

$$\begin{pmatrix} i\partial_t + \nabla^2 + L_i(|E_0|^2) & h_i(t) \\ h_i^*(t) & -i\partial_t + \nabla^2 + L_i(|E_0|^2) \end{pmatrix} \times \begin{pmatrix} \delta E \\ \delta E^* \end{pmatrix} = 0, \tag{2.3}$$

where

$$L_i(|E_0|^2) = F(|E_0|^2) + F'(a)|_{a=|E_0|^2}|E_0|^2 (a \equiv |E|^2), \tag{2.4}$$

$$h_i(t) = F'(a)|_{a=|E_0|^2} E_s^2(t).$$

On the other hand, we can obtain the relation of the linear growth rate with the instability wave number by using the standard method [29,30]

$$\gamma(K_A) = K_A[E_0F'(E_0) - K_A^2]^{1/2}, \tag{2.5}$$

where $K_A \equiv K$ for the case of one dimension and $K_A = \sqrt{\mathbf{K}_\perp \cdot \mathbf{K}_\perp} = \sqrt{K_X^2 + K_Y^2}$ for the case of two dimensions, and K, K_X, and K_Y are the wave numbers of the modulational instabilities to the uniform solution in the one-dimensional space and the two-dimensional space, respectively.

Considering the periodic boundary condition, for Eq. (2.3), we can define the eigenfunction as

(i) the case of one dimension:

$$\begin{pmatrix} \delta E \\ \delta E^* \end{pmatrix} = \begin{pmatrix} \epsilon e^{i\lambda t} \\ \epsilon^* e^{-i\lambda^* t} \end{pmatrix} \cos(KX); \tag{2.6}$$

(ii) the case of two dimensions:

$$\begin{pmatrix} \delta E \\ \delta E^* \end{pmatrix} = \begin{pmatrix} \epsilon e^{i\lambda t} \\ \epsilon^* e^{-i\lambda^* t} \end{pmatrix} \cos(K_X X)\cos(K_Y Y), \tag{2.7}$$

where ϵ and ϵ^* are small parameters. In this work, we choose the wave number to be that corresponding to the maximum growth rate, that is, $K_{\max} = \sqrt{\frac{1}{2}E_0F'(E_0)}$ for the one-dimensional space and $K_{X,\max} = K_{Y,\max} = \frac{1}{2}\sqrt{E_0F'(E_0)}$ for two-dimensional space.

Inserting Eq. (2.6) or Eq. (2.7) into Eq. (2.3), we obtain the equation of eigenvalue:

$$\lambda^2 - 2\omega_s\lambda - A^2 + 2\omega_s A - E_0^2 = 0, \tag{2.8}$$

where $A = -K_A^2 + L_i(|E_0|^2)$.

B. Initial conditions

According to Eq. (2.2) and Eq. (2.6) or Eq. (2.7), we can choose the initial condition in the numerical experiments to be

(i) the case of one dimension:

$$E(X,0) = E_0 + \epsilon e^{i\theta}\cos(KX); \tag{2.9}$$

(ii) the case of two dimensions:

$$E(X,Y,0) = E_0 + \epsilon e^{i\theta}\cos(K_X X)\cos(K_Y Y). \tag{2.10}$$

C. Phase space

For the continuum Hamiltonian system (1.1), an available choice of the phase space is also a key problem to analyze the dynamic behaviors due to the existence of the infinite degrees of freedom. From Eq. (2.8), we note that E_0 would correspond to the saddle point if there were a pair of conjuge complex roots for eigenvalue λ, that is, $\lambda = \alpha \pm i\beta$. To further illustrate this problem, we should discuss some models in detail. Without loss of generality, we assume $\omega_s \equiv 1$ and finally obtain the following.

(i) For model (1.6) (the case of $q = 1$),

$$L_1 = 2|E_0|^2, \quad h_1 = E_s^2(t),$$

$$K_{\max} = E_0, \quad K_{X,\max} = K_{Y,\max} = \tfrac{1}{\sqrt{2}}E_0, \tag{2.11}$$

$$\lambda = 1 \pm i,$$

for $E_0 = 1$.

(ii) For model (1.7),

$$L_2 = 2|E_0|^2 - 3g|E_0|^4, \quad h_2 = E_s^2(t)(1 - 2g|E_0|^2),$$

$$K_{\max} = E_0(1 - 2gE_0^2)^{1/2},$$

$$K_{X,\max} = K_{Y,\max} = \frac{1}{\sqrt{2}}K_{\max}, \tag{2.12}$$

$$\lambda = 1 \pm i\frac{-1 + 4g + \sqrt{1 - 4g}}{2g},$$

for $E_0 = \sqrt{\frac{1-\sqrt{1-4g}}{2g}}$ with $0 \le g < 1/4$.

(iii) For model (1.8),

$$L_3 = \frac{2|E_0|^2 + g|E_0|^4}{(1 + g|E_0|^2)^2}, \quad h_3 = \frac{E_s^2(t)}{(1 + g|E_0|^2)^2},$$

$$K_{\max} = \frac{E_0}{1 + gE_0^2}, K_{X,\max} = K_{Y,\max} = \frac{1}{\sqrt{2}}K_{\max}, \tag{2.13}$$

$$\lambda = 1 \pm i(1 - g),$$

for $E_0 = \sqrt{\frac{1}{1-g}}$ with $0 \le g < 1$.

(iv) For model (1.9),

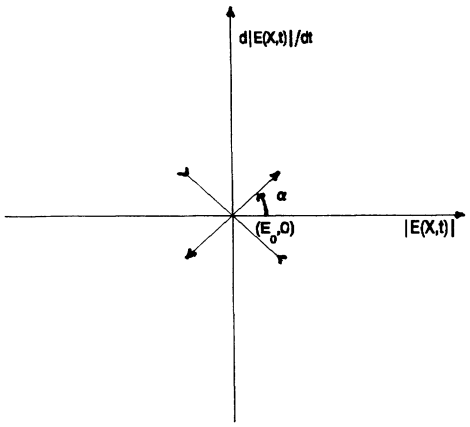

FIG. 1. Local phase flows of saddle point $(E_0, 0)$, which are obtained in terms of Eqs. (2.13) and (2.15), and where $\alpha = 1 - g$.

$$L_4 = \frac{1}{2g}[1 - (1 - 2g|E_0|^2)e^{-2g|E_0|^2}],$$

$$h_4 = E_s^2(t)e^{-2g|E_0|^2},$$

$$K_{\max} = E_0 e^{-gE_0^2}, \quad K_{X,\max} = K_{Y,\max} = \frac{1}{\sqrt{2}}K_{\max}, \tag{2.14}$$

$$\lambda = 1 \pm i\frac{1-2g}{2g}\ln(1-2g),$$

for $E_0 = \sqrt{\frac{1}{2g}\ln(1-2g)^{-1}}$ with $0 \le g < 1/2$.

Therefore, we have that (a) in the case of one dimension

$$|\delta E| = c_1\cos(K_{\max}X)e^{\beta t} + c_2\cos(K_{\max}X)e^{-\beta t},$$

$$\frac{d|\delta E|}{dt} = c_1\beta\cos(K_{\max}X)e^{\beta t} - c_2\beta\cos(K_{\max}X)e^{-\beta t}; \tag{2.15}$$

(b) in the case of two dimensions

$$|\delta E| = c_1\cos(K_{X,\max}X)\cos(K_{Y,\max}Y)e^{\beta t} + c_2\cos(K_{X,\max}X)\cos(K_{Y,\max}Y)e^{-\beta t},$$

$$\frac{d|\delta E|}{dt} = c_1\beta\cos(K_{X,\max}X)\cos(K_{Y,\max}Y)e^{\beta t} - c_2\beta\cos(K_{X,\max}X)\cos(K_{Y,\max}Y)e^{-\beta t}; \tag{2.16}$$

and

$$\left.\frac{\delta E}{\delta E^*}\right|_{t=0} = \pm i. \tag{2.17}$$

Thus we can construct the phase space as $(|\delta E|, d|\delta E|/dt)$ or $(|E|, d|E|/dt)$. Obviously, the point $(E_0, 0)$ in phase space $(|E|, d|E|/dt)$ corresponds to the hyperbolic fixed point. Comparing initial condition Eq. (2.9) or Eq. (2.10) with Eq. (2.17), we easily determine that the unstable manifolds for possessing the hyperbolic fixed point correspond to $\theta = 45°$ and $225°$, and the stable manifolds correspond to $\theta = 135°$ and $315°$ (see Fig. 1).

III. THE INTEGRABILITY OF THE ONE-DIMENSIONALLY CUBIC NSE

To better discuss the pattern dynamics of Eq. (1.1), we should simply describe the dynamic characteristics of the well-known cubic NSE. For convenience, we write the cubic NSE in an obvious form:

$$i\partial_t E + \partial_{XX}E + |E|^2E = 0. \tag{3.1}$$

In Sec. II, we have shown that $(1, 0)$ in the phase space corresponds to a saddle point. If we take $\theta = 45°$ in the initial condition (2.9), the orbit that possesses the saddle point $(1, 0)$ corresponds to the homoclinic orbit (HMO) [19,31]. If we consider $\theta \neq 45°$, then the orbit should deviate from the HMO. Considering the integrability of the cubic NSE, on the other hand, we have that these orbits must be the exact recurrent solutions [11].

In the following, we turn to the numerical experiments. Here, the standard splitting-step spectral method [32] has been improved in order to increase the accuracy of conserved quantities. For the one-dimensional problem, the periodic length of the system is taken as $L = 2\pi/K_{\max}$. For the two-dimensional problem that will be discussed in Sec. V, the periodic lengths of the system are chosen as $L_X = 2\pi/K_{X,\max}$ and $L_Y = 2\pi/K_{Y,\max}$, respectively.

A. Homoclinic connection

In the initial condition, we take $\theta = 45°$ and $225°$, respectively. To determine the stable and unstable manifolds for the hyperbolic fixed point $(1, 0)$, we trace the unstable manifold by considering $t > 0$ and measure the stable manifold by simulating $t < 0$. Figure 2 is our computational result, which is traced at $X = 0$. From Fig. 2, we observe that the stable manifold $W^{(s)}$ smoothly joins with the unstable manifold $W^{(u)}$, that is, $W^{(s)}(\mathbf{X}^*) = W^{(u)}(\mathbf{X}^*)$ $[\mathbf{X}^* \equiv (1, 0)]$. This structure is called a homoclinic connection. The orbit that possesses the saddle point $(1, 0)$ corresponds to the HMO. As far as a finite dimensional dynamic system is concerned, the stable and unstable orbits for the hyperbolic fixed point would be smoothly joined to each other if the unperturbed system was taken to be integrable. For the cubic NSE, it is illustrated in Fig. 2 that such an idea is still effective for us to analyze the integrability of the continuum Hamiltonian system. Of course, almost any nonintegrable perturbation may destroy the connection. In the following section, we will again discuss such a problem for the saturable NSE (1.1).

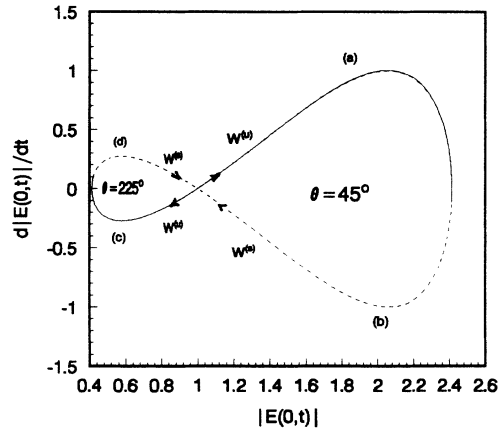

FIG. 2. Stable $W^{(s)}$ and unstable $W^{(u)}$ manifolds for the hyperbolic fixed point $(E_0, 0)$ with $\theta = 45°$ and 225°, where the solid curve is computed with $t > 0$, and the dashed curve is computed with $t < 0$.

B. Recurrence

1. Periodic trajectory

Because of the integrability of the cubic NSE, its solutions can be displayed in terms of a class of periodic solutions. For our initial condition (2.9), Yuen and Ferguson [11] showed that the evolution of fields should be "simple." In other words, the solution developed by modulational instability corresponds to an exactly periodic solution (see Fig. 3).

It is noted from Fig. 3 that different trajectories are exhibited when we vary the initial phase θ. In numerical simulations, we find that the value of the amplitude for fields is larger than the value 1 as seen in Fig. 3(a) for $0 \leq \theta < 45°$, and the value periodically oscillates within the regions of 0 and 2.6 as shown in Fig. 3(b) for $45° < \theta \leq 90°$. For phase-space trajectories, Fig. 3(c) exhibits a clearer picture. When $\theta = 45°$, the trajectory that possesses the hyperbolic fixed point $(1, 0)$ is of the periodic motion around an elliptic fixed point. When $\theta = 0°$, the trajectory that deviates from the hyperbolic fixed point $(1, 0)$ periodically moves around the same elliptic fixed point as that for $\theta = 45°$. When $\theta = 90°$, however, the trajectory is of the periodic motion around two elliptic fixed points and the hyperbolic point $(1, 0)$. For these pictures, of course, the perturbation parameter ϵ in the initial condition should be quite small. If ϵ is not small, there could be some difference between theoretical results and numerical ones for our determining the region of θ.

2. Spatially coherent patterns

As mentioned above, we understand that the integrability of the one-dimensionally cubic NSE can be de-

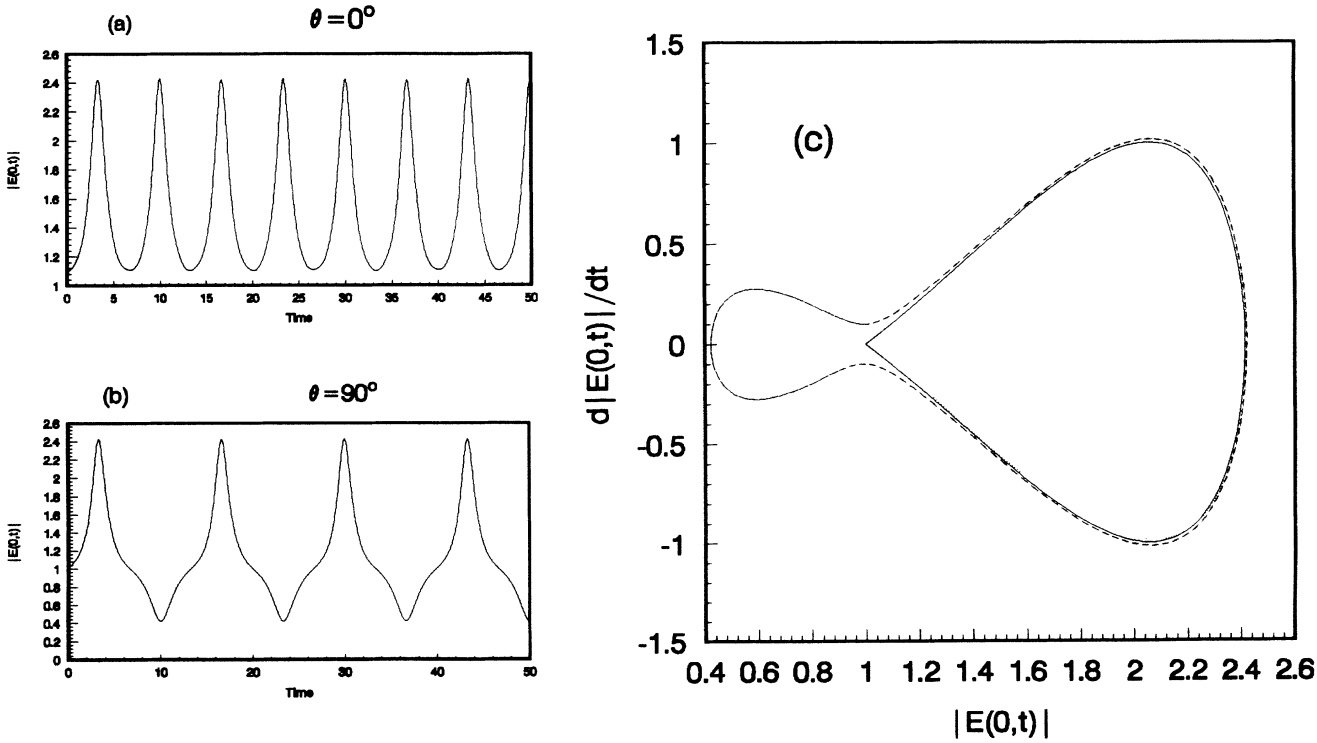

FIG. 3. Solutions of the one-dimensionally cubic NSE. (a) and (b) correspond to the amplitude of fields for $\theta = 0°$ and 90°; (c) is the phase-space trajectories, where the dotted line corresponds to $\theta = 0°$, the solid line corresponds to $\theta = 45°$, and the dash line is $\theta = 90°$.

scribed in terms of strictly periodic trajectories. As a matter of fact, such an integrability is also associated with the well-known FPU recurrence. For our simply recurrent initial condition, the evolution of the spatially coherent patterns as shown in Fig. 4 exhibits an exactly periodic recurrent solution.

Particularly, Fig. 4(a) and Fig. 4(b) represent two types of patterns. In other words, a structure similar to that plotted in Fig. 4(a) will appear for $0 \leq \theta \leq 45°$, and one similar to that described in Fig. 4(b) will be formed for $45° < \theta \leq 90°$. Comparing Fig. 3 with Fig. 4, we easily understand that the choice process of these patterns depends on the phase-space manifolds. If the trajectory only recurs around an elliptic point [Fig. 3(a)], then pattern Fig. 4(a) will be formed. If the trajectory moves around two elliptic points and the hyperbolic fixed point $(1,0)$ [Fig. 3(b)], then the pattern Fig. 4(b) will be produced. Considering the Hamiltonian perturbation that is added in the cubic NSE, in the following sections, one can observe that the stochastic choice of these patterns is associated with the irregular HMO crossings.

3. Evolution of energy spectrum

To display this recurrence, we further measure the evolution of the energy contained in the Fourier modes. In Fourier space, we define the energy of the system as

$$H = \sum_n H_{K_n} = \sum_n |E_{K_n}|^2. \tag{3.2}$$

In our experiment, the initial energy is added to the mode $K_{\max}$. From Fig. 5, we observe that a large part of the energy in the system lies in the first and second modes. The temporal evolution of the energy in all modes is periodic, which is consistent with the periodic recurrence solution [Figs. 3 and 4]. In a sense, the unstable modulation to the uniform solution would first grow at an exponential rate as predicted by Benjamin and Feir [33], but eventually the solution would demodulate and return to a near-uniform state.

On the other hand, the periodically evolving process of the energy in Fourier modes is associated with the spatially coherent structures. That is, the amplitude of soliton structures is dominated by the total energy of the system, while the width and the pattern of the coherent structures are associated with the energy partition in the high modes. Thus, solitons developed by modulational instability keep their spatially coherent patterns and temporally periodic evolutions. The integrability of the one-dimensionally cubic NSE can also be described in terms of the exactly periodic recurrence in the energy space.

IV. SPATIOTEMPORAL CHAOS IN ONE-DIMENSIONAL SPACE

In the case of one dimension, the Hamiltonian of the NSE (1.1) can be rewritten as

$$H = H_0 + H_1, \tag{4.1}$$

where

$$H_0 = \int (|E_X|^2 - \tfrac{1}{2}|E|^4) dX, \tag{4.2}$$

$$H_1 = \int [\tfrac{1}{2}|E|^4 - f(|E|^2)] dX. \tag{4.3}$$

In Sec. III, we obviously illustrate that the integrability of Hamiltonian H_0 can be described in terms of the homoclinic connection of the periodic trajectories. Is the Hamiltonian perturbation H_1 integrable or nonintegrable? As yet, one has still not referred to a quite satisfactory theory to deal with these problems, especially on the integrability of the continuum Hamiltonian system. Generally speaking, there may exist finite solitons for integrable systems, such as the Langmuir soliton in the cubic NSE. However, the existence of a solitary

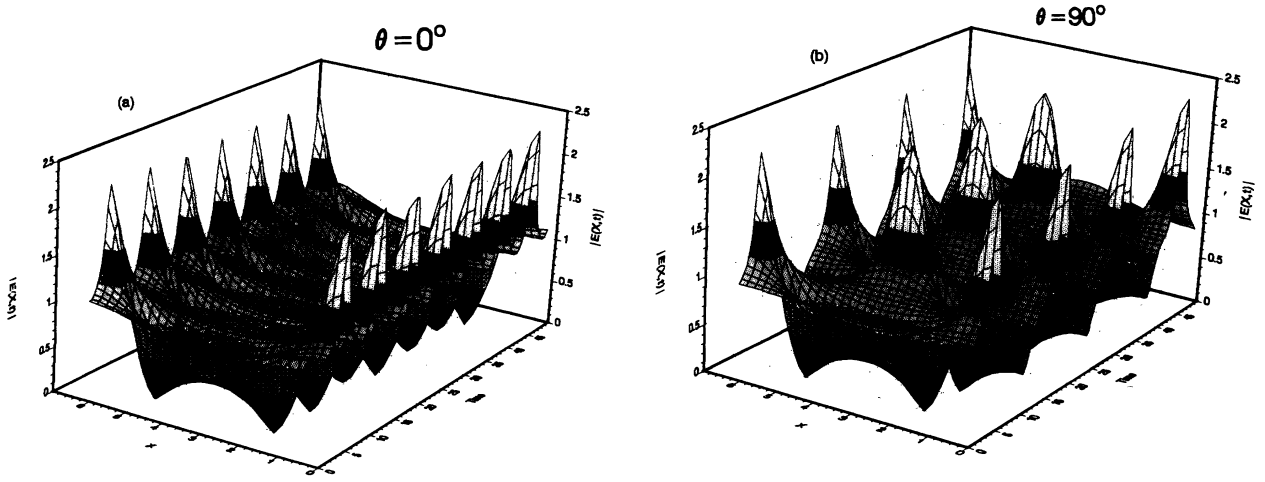

FIG. 4. The coherent structures of the one-dimensionally cubic NSE; (a) and (b) correspond to $\theta = 0°$ and $90°$, respectively.

cannot show the system to be integrable unless we can constitute a Lax pair. For example, there exists a standard Langmuir solitary for the model (1.6) [19], but the propagation of fields displays a typically chaotic characteristic. Here we numerically discuss the integrablility problem of the NSE (1.1).

A. Irregular HMO crossings

Taking into account Eq. (1.1) and Eqs. (1.6)–(1.9), we know that these NSE's correspond to the integrable equations when $g = 0$, and the stable and unstable manifolds that possess the saddle point $(1, 0)$ are smoothly joined to each other. Making use of the results obtained in linear stability analyses, we also choose the initial parameters as $\theta = 45°$ and $g = 0.1$, and measure their characteristics of the stable and unstable manifolds for models (1.7)–(1.9), respectively.

From Fig. 6, we obviously observe that the stable and unstable manifolds in the phase space do not smoothly join together, which illustrates that these saturable NSE's are nearly integrable [31,34]. Comparing our simulation results (Fig. 6) with those in finite dimensional Hamiltonian systems [34], it is also noted that there are not an infinite number of homoclinic points in Fig. 6. As for the finite dimensional system, the fact that one transverse homoclinic point implies an infinity

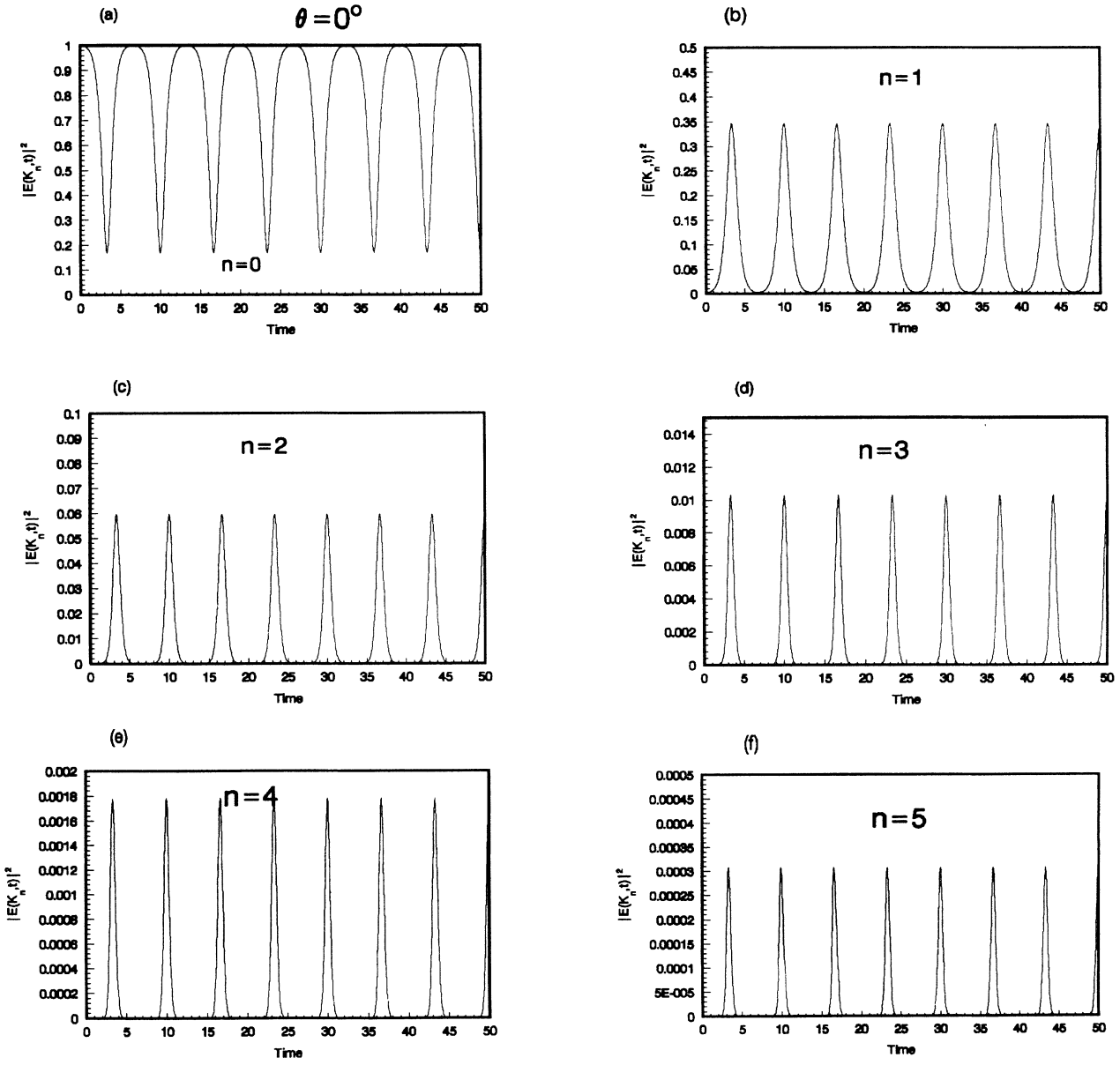

FIG. 5. The energy evolution in the first six Fourier modes for the one-dimensionally cubic NSE.

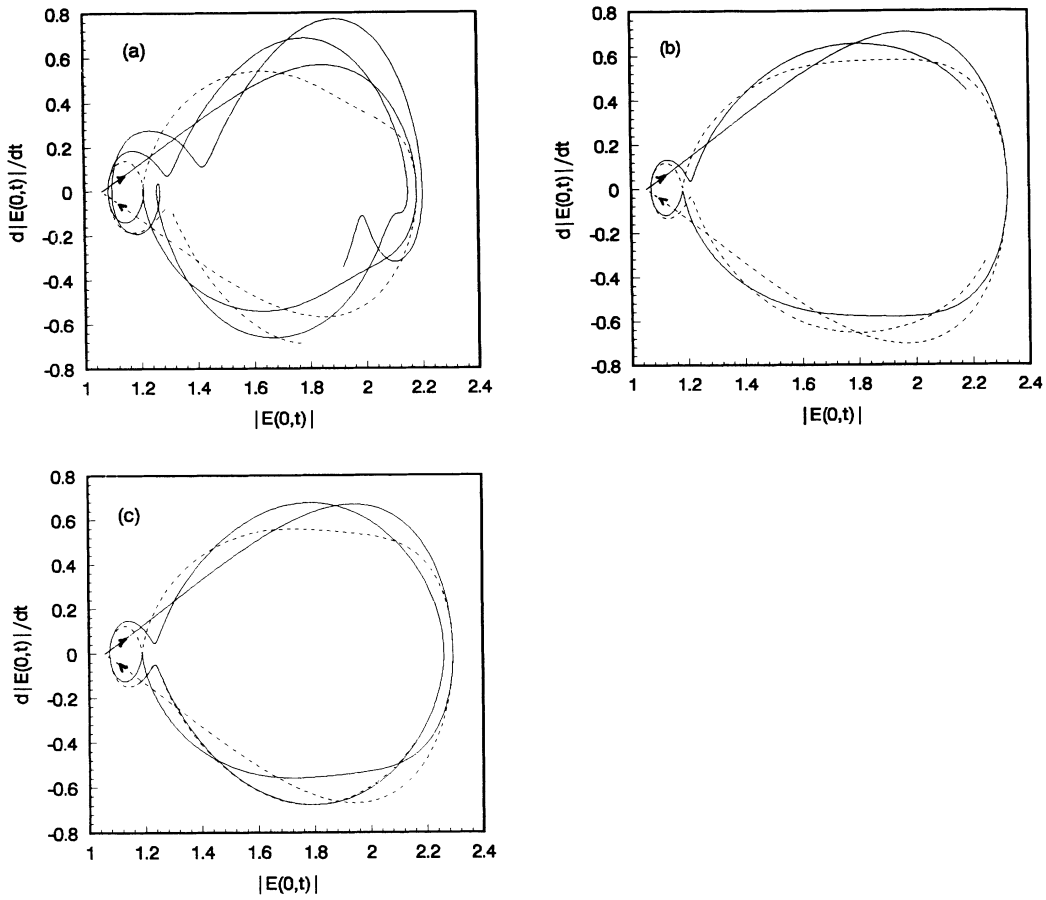

FIG. 6. Stable and unstable manifolds for the hyperbolic fixed point $(E_0, 0)$ with $\theta = 45°$, where (a), (b), and (c) correspond to the models (1.7), (1.8), and (1.9), respectively.

of homoclinic points leads to extreme stretching and folding of the manifolds. However, we notice that our phase space $(|E(X,t)|, d|E(X,t)|/dt)$ is only the projection of a high-dimensional space, where the information about phase for wave fields is not considered. Therefore, there may exist some difference between our HMO crossings and those in a finite dimensional Hamiltonian system in which infinite homoclinic points appear.

We also observe from Fig. 6(a)–Fig. 6(c) that their topologic structures are basically consistent. In a sense, the Hamiltonian perturbation H_1 (4.3) destroys the homoclinic connection and leads to the destruction of the integrability.

B. Spatiotemporal chaos

1. Quasi-periodic route to chaos

As stated above, we know that the high order Hamiltonian perturbation can result in the formation of irregular HMO crossings. We recall that the infinite periodic homoclinic states act, under perturbation, as sources of sensitivity (including chaos). Therefore, we should further discuss the chaotic characteristics and route.

We do not give a detailed description on all dynamic models as mentioned in Sec. I. As a specific example, we only deal with the model (1.8), which is rewritten as

$$i\partial_t E + \partial_{XX} E + \frac{|E|^2}{1 + g|E|^2} E = 0. \tag{4.4}$$

In numerical processes, we choose the initial parameters as $\epsilon = 0.1$, $\theta = 1.0005\pi/4$, and vary g.

After many experiments, we find that the route from the exactly periodic solution to chaos is a quasiperiodic route as shown in Fig. 7. From the figure, we see that the periodic oscillation of amplitude for fields is broken down with the increase of g; in particular, the stochastic behavior occurs as displayed in Fig. 7(d) for $g = 0.1$. For the phase-space trajectories, an exactly recurrent motion for the cubic NSE ($g = 0$) is given in Fig. 7(a) and Fig. 7(a′). We also note that the phase trajectories in Fig. 7(a′) only move around an elliptic fixed point, and are not completely consistent with those discussed in Sec. III (B). This is because the initial parameter ϵ is not quite small. For $g = 0.0005$, the figures [Fig. 7(b)

and Fig. 7(b′)] of phase space behave like the quasirecurrent solution where the trajectory is not the exactly periodic one. For $g = 0.005$, Figs. 7(c)–7(c″) show that more subharmonics appear. Comparing Fig. 7(b) with Fig. 7(c), we see that the amplitude of the wave fields for the case of $g = 0.005$ is more irregular; especially the trajectories of the phase space Fig. 7(c′) illustrate that the KAM tori become thicker but are not completely destroyed. Figure 7(c″) shows that more frequencies are produced due to the increase of the saturable nonlinearity. For $g = 0.1$, the irregular homoclinic orbit crossings are also drawn in Fig. 7(d′). To describe the route, a better technique is to measure the power spectrum. The foundation frequency of the periodic solution for the cubic NSE is labeled in Fig. 7(a″). Also, Fig. 7(d″) indicates the noiselike characteristic typical of chaotic time evolution. It is particularly noted that Fig. 7(b″) exhibits a quasiperiodic spectrum [34,35], where two incommensurate frequencies $\{\omega_0, \omega_1\}$ appear, and $\omega_2 = \omega_0 - \omega_1$. In the numerical simulations, we find that such a standard spectrum is sensitively dependent on the initial parameters, such as θ and g. In general, more subharmonics [as described in Fig. 7(c″)] may be observed with variation of the parameters [36]. Hence we can conclude the route is as follows: *period* (coherent structures) $\{\omega_0\} \rightarrow$ *quasiperiod* $\{\omega_0, \omega_1\}$ (pseudorecurrence) $\rightarrow$ *subharmonics* $(\omega_0, \omega_1, \ldots, \omega_n) \rightarrow$ *chaos* (spatiotemporal complexity).

Speaking in terms of physics, the Hamiltonian perturbation

$$H_1 = \int \left\{ \tfrac{1}{2}|E|^4 - \left[\frac{1}{g}|E|^2 - \frac{1}{g^2}\ln(1 + g|E|^2) \right] \right\} dX \tag{4.5}$$

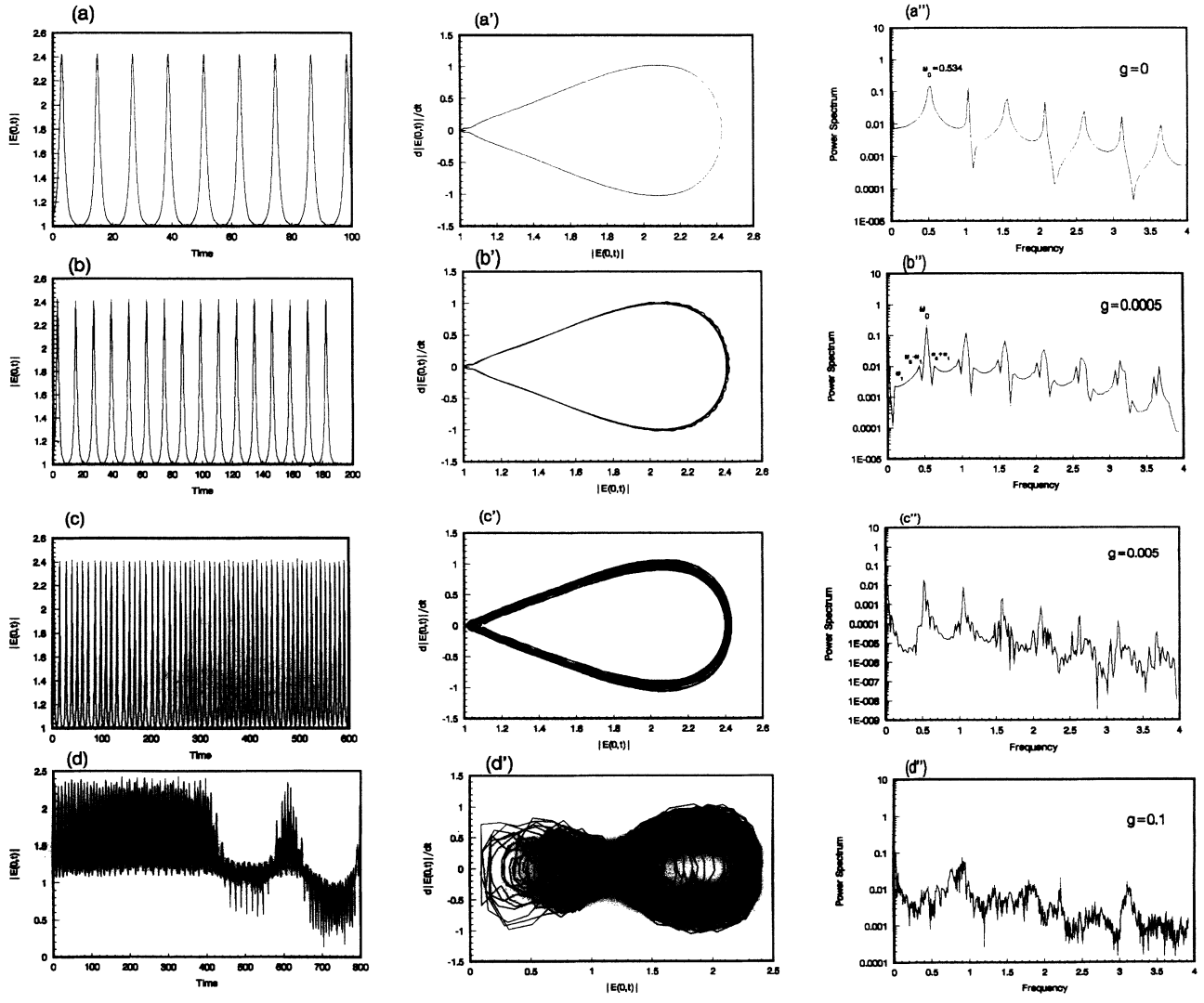

FIG. 7. The solutions of Eq. (4.4) with $\epsilon = 0.1$ and $\theta = \frac{1.0005\pi}{4}$, where a fixed position ($X = 0$) is traced. (a), (b), (c), and (d) correspond to the temporal evolution of amplitude for fields; (a′), (b′), (c′), and (d′) are the structures of phase space, noting that (d′) indicates the irregular homoclinic orbit crossings; (a″), (b″), (c″), and (d″) represent the power spectra corresponding to (a), (b), (c), and (d), respectively. In particular, (b′) exhibits the quasiperiodic spectrum.

drives the formation of stochastic fields and the destruction of recurrence. When $g = 0$, the trajectory is periodic and the spatial patterns are coherent due to the integrability of the system. When g is quite small, a periodic trajectory becomes the quasiperiodic one. With further increase of g, the nonintegrable Hamiltonian perturbation H_1 drives the KAM tori and the coherent structures to be completely broken down.

2. *Spatially complicated patterns*

We have understood that nonintegrable perturbation leads to the chaotic propagation of wave fields. On the other hand, we observe from Fig. 8 that the solitonlike structures are still kept but are quite irregular. The appearance of these complicated patterns means that the exactly recurrent structures disappear. In fact, the stochastic choice of these patterns is associated with the irregular HMO crossings. Comparing Fig. 7(d′) with Fig. 8, one can easily understand that these two similar kinds of patterns as described in Fig. 4(a) and Fig. 4(b) may also be formed under the current parameters. In addition, these irregular patterns depend on the partition of the energy in the Fourier modes. For the coherent structures (Fig. 4), the energy in the Fourier modes represents homogeneous decay. For these spatiotemporally complicated patterns (Fig. 8), however, the partition of the energy in the Fourier modes represents inhomogeneous decay [35]. To better analyze the mechanism by which complicated patterns are formed, we should also discuss the processes of evolution of the energy contained in the Fourier modes.

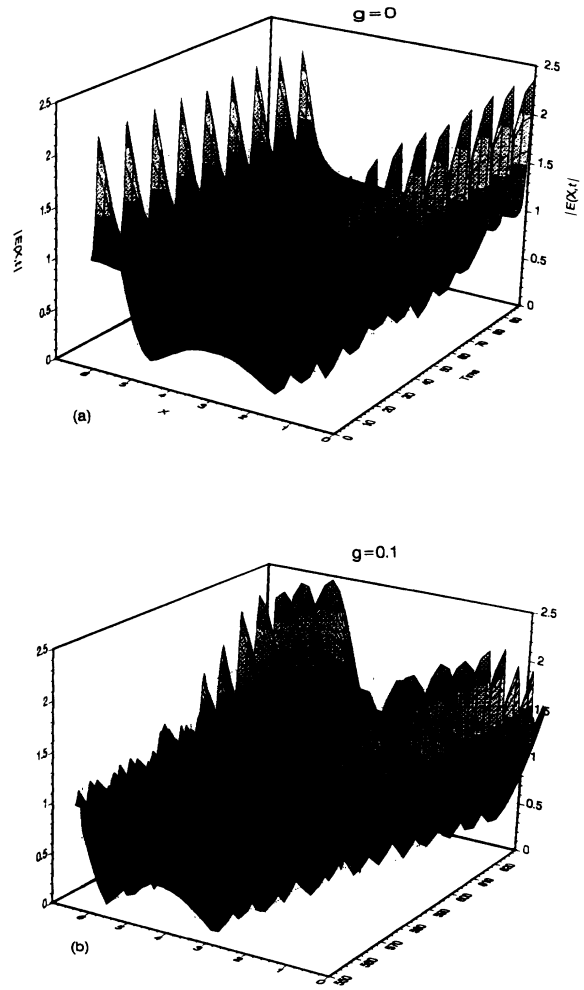

FIG. 8. The spatiotemporal patterns for the saturable NSE (4.4) with $\epsilon = 0.1$ and $\theta = \frac{1.0005\pi}{4}$, but the value g changed. (a) Coherent patterns with $g = 0$; (b) spatiotemporally complicated patterns with $g = 0.1$.

3. *Stochastic evolution of energy spectrum*

The evolution of energy in the first four Fourier modes is described in Fig. 9. Obviously, a large part of the energy in the system still lies in the low Fourier modes. As for the first two modes, the evolution of the energy behaves like a quasiperiodic motion, which makes sure the spatially localized structures (Fig. 8) are still kept. However, the evolution of the energy in the high modes exhibits a stochastic behavior, which illustrates spatial patterns that are very irregular as seen in Fig. 8. Physically, the energy in the system, which is initially confined to the master mode, would spread to many slave harmonic modes because of the nonlinear interaction, but would not regroup into the original lowest mode. The stochastic evolution of the energy in the Fourier modes, in which the slave modes interact with the master one, leads to the formation of spatiotemporal chaos.

V. PATTERN STRUCTURES IN TWO-DIMENSIONAL SPACE

In this section, we turn to discussing the dynamic characteristics of the two-dimensional NSE. Also we only deal with the model (1.8) which is clearly written as follows:

$$iE_t + \nabla^2 E + \frac{|E|^2}{1 + g|E|^2} E = 0. \tag{5.1}$$

For this model, Akhemediev *et al.* [22] showed numerically that pseudorecurrence can appear in two-dimensionally modulational instability. Moreover, the singular solution can also exist [23]. As we know, however, spatiotemporal dynamics in two-dimensional space has not been systematically studied as yet, especially the spatial patterns and the chaotic characteristics.

Here, we further investigate the behaviors of the solution in terms of the modulational instability in two-dimensional space. First, we write the linear growth rate (2.5) as the following obvious form:

$$\gamma(K_\perp) = K_\perp \left[\frac{2gE_0^2}{(1 + gE_0^2)^2} - K_\perp^2 \right]^{1/2}, \tag{5.2}$$

where $K_\perp = \sqrt{K_X^2 + K_Y^2}$, which is sketched in Fig. 10.

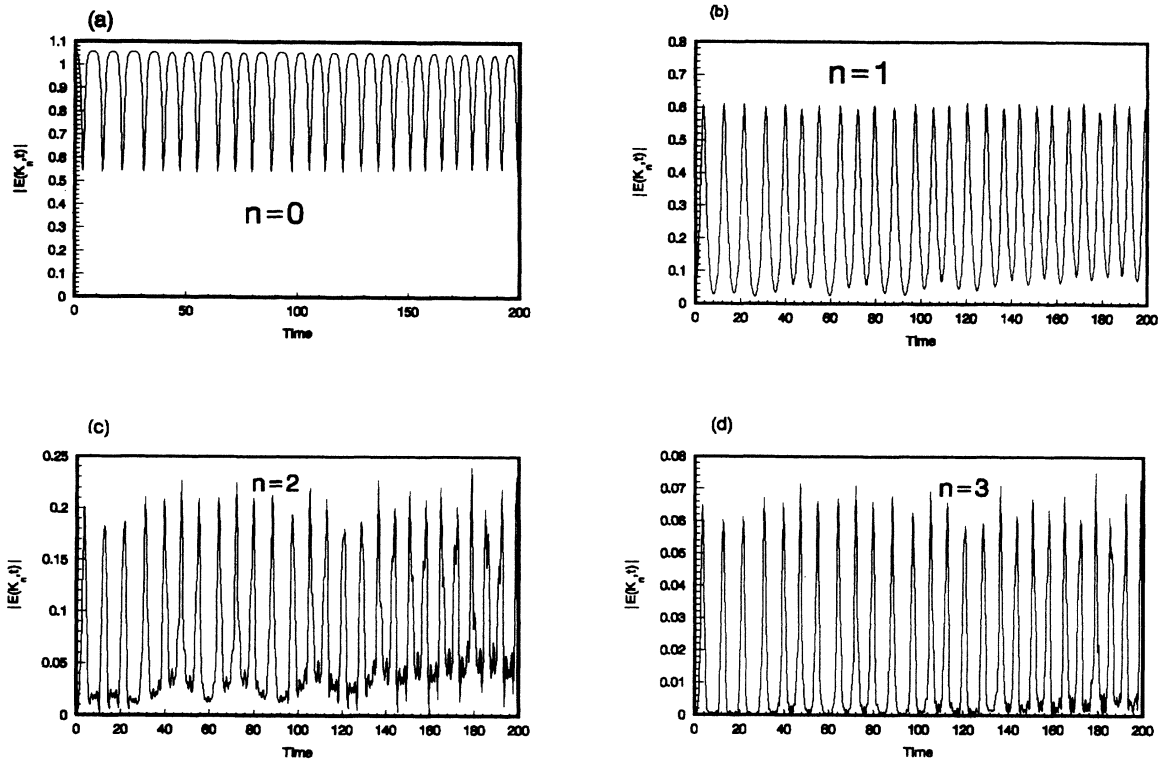

FIG. 9. The energy evolution in the first four Fourier modes for the NSE (4.4), where the parametric values correspond to those in Fig. 7(d).

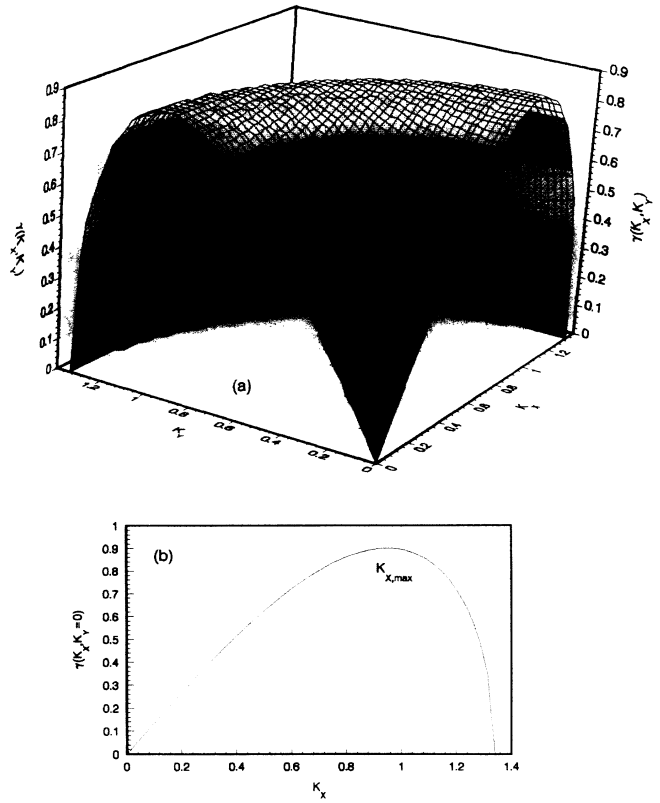

FIG. 10. (a) The linear growth rate vs K_X and K_Y. (b) The growth rate vs K_X with $K_Y = 0$.

A. Irregular HMO crossings

From Eqs. (2.16) and (2.17), we know that $(E_0, 0)$, where $E_0 = [1/(1-g)]^{1/2}$ with $0 \leq g < 1$, corresponds to a saddle point in the phase space $(|E(X,Y,t)|, d|E(X,Y,t)|/dt)$. The stable and unstable manifolds that possess the saddle point also correspond to $\theta = 45°, 225°$ and $\theta = 135°, 315°$, respectively. As discussed in Sec. IV, here, we choose the parametric values as $\theta = 45°$, $g = 0.1$, and trace the trajectories at the fixed space point $X = 0$ and $Y = 0$. From Fig. 11, we observe that the phase-space trajectories are completely similar to that in the case of one dimension as shown in Fig. 6. Therefore, we can say that the formation of chaos in the current two-dimensional space is also due to irregular HMO crossings. Of course, we cannot think that such a HMO chaos in the saturable NSE (5.1) only arises from the nonlinear perturbation. This is because the cubic NSE in two-dimensional space is also not integrable. In the following analyses, we may understand that the pseudorecurrence appears if the saturable nonlinear effects are very strong. With the decrease of the saturable effects, the irregular HMO crossings lead to the destruction of pseudorecurrence and the appearance of stochasticity for fields.

B. Blowup, chaos, and pseudorecurrence

In the following simulations, we choose parametric values as $\epsilon = 0.1$ and $\theta = \frac{1.0005\pi}{4}$, and vary the g value.

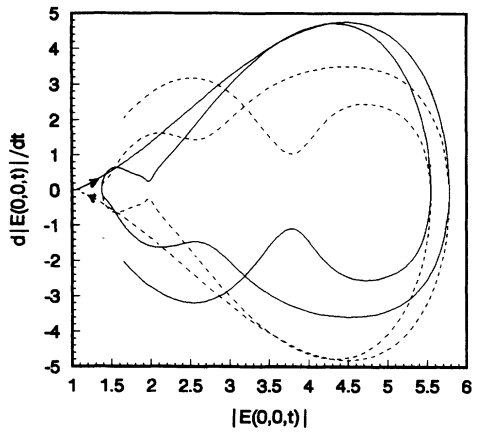

FIG. 11. Stable and unstable manifolds for the hyperbolic fixed point $(E_0, 0)$ in the two-dimensional NSE (5.1); it is noted that this structure is similar to that in the case of one dimension, which illustrates the characteristic of HMO chaos.

1. Singular solution

To clearly study the features of the dynamic system (5.1), we first discuss characteristics of the two-dimensionally cubic NSE. As $g = 0$, Eq. (5.1) corresponds to the critical NSE. The solution should be the singular one, where the time of blowup is finite [23] and the field intensities exhibit catastrophic processes.

In order to describe the temporally evolutive characteristics in more detail, we trace the trajectory at a fixed position, i.e., $X = 0, Y = 0$. Figure 12(a) exhibits the time evolution of amplitude for fields, where the solution is rapidly developed from the initial value 1 to the larger value within a finite time that is associated with the time of blowup as seen from Fig. 13. Owing to the rapid change of amplitude with time, its slope must be very large. Therefore, Fig. 12(b) indicates that the trajectory in phase space is not bounded within a small area.

2. Chaotic solution

Taking into account $g = 0.1$, we observe that the amplitude stochastically oscillates as shown in Fig. 12(c). The field E_0 is developed due to the modulational instability from the initial value E_0 to a finite amplitude toward saturation, then oscillates down because of the saturable nonlinear force (ponderomotive force), and so on. For the trajectory, its manifolds exhibit irregular HMO crossings, where the trajectory as seen in Fig. 12(d) is bounded with a finite region of phase space. Thus our simulation indeed verifies the prediction given by Akhemediev *et al.* [22] on HMO chaos.

3. Pseudorecurrent solution

A more interesting phenomenon is observed in Fig. 12(e)–Fig. 12(h). With the increase of parameter g, we find that pseudorecurrence appears. As plotted in Fig. 12(e) and Fig. 12(g), the amplitude of the fields behaves like a periodiclike oscillation. These phase trajectories are basically regular, where the motion is smooth in small regions of phase space as described in Fig. 12(f) and Fig. 12(h). In other words, the KAM tori are not completely broken down when the parameter g comes close to 1. In the work of Akhemediev *et al.* [22], they chose $g = 1$ and also observed such a pseudorecurrent behavior.

C. Spatial patterns

In the following, we describe the pattern structures corresponding to these three kinds of solutions as stated in the above. For the case of $g = 0$, we observe from Fig. 13(a)–Fig. 13(d) the developing processes of the initial field (2.10) due to the modulation instability. Figure 13(c) and Fig. 13(d) correspond to the singular solutions. Comparing Fig. 13(b) with Fig. 13(c), we understand that the time of blowup lies in the regions of $t^* = 1.2 - 2.0$. With the evolution of time, the solution is rapidly contracted and the energy of the system is concentrated on some small spots. In laser-produced plasmas, these processes describe filamentation of laser beams [25–27,37] as the time variable t is replaced by the propagative distance Z. In plasma turbulence, they describe the Langmuir collapse due to the ion-acoustic perturbation [8], which is influenced by ponderomotive force in the NSE (1.1).

For the case of the chaotic solution, the numerical experiments show that the singular solution does not occur where the saturable nonlinear effects prevent blowup of the solution. Speaking in terms of physics, the saturable nonlinear force prevents the collapse of Langmuir waves or the concentration of energy. We find from Fig. 14 that different patterns are formed. In particular, the spatial symmetry is broken down with the development of wave fields as sketched in Fig. 14(b), which are different from those in the initial stages of evolution where the spatial symmetry is kept as shown in Fig. 14(a). For these structures, we will now give a description in terms of the energy spectrum.

For the case of pseudorecurrent solutions, we see from Fig. 15 where $g = 0.8$ that the spatial structures at $t = 50$ are different from those at $t = 200$; however, the symmetry of the solution is basically kept. In addition, we note from Fig. 16 where $g = 0.98$ that the spatial structure at $t = 50$ is basically consistent with that at $t = 200$.

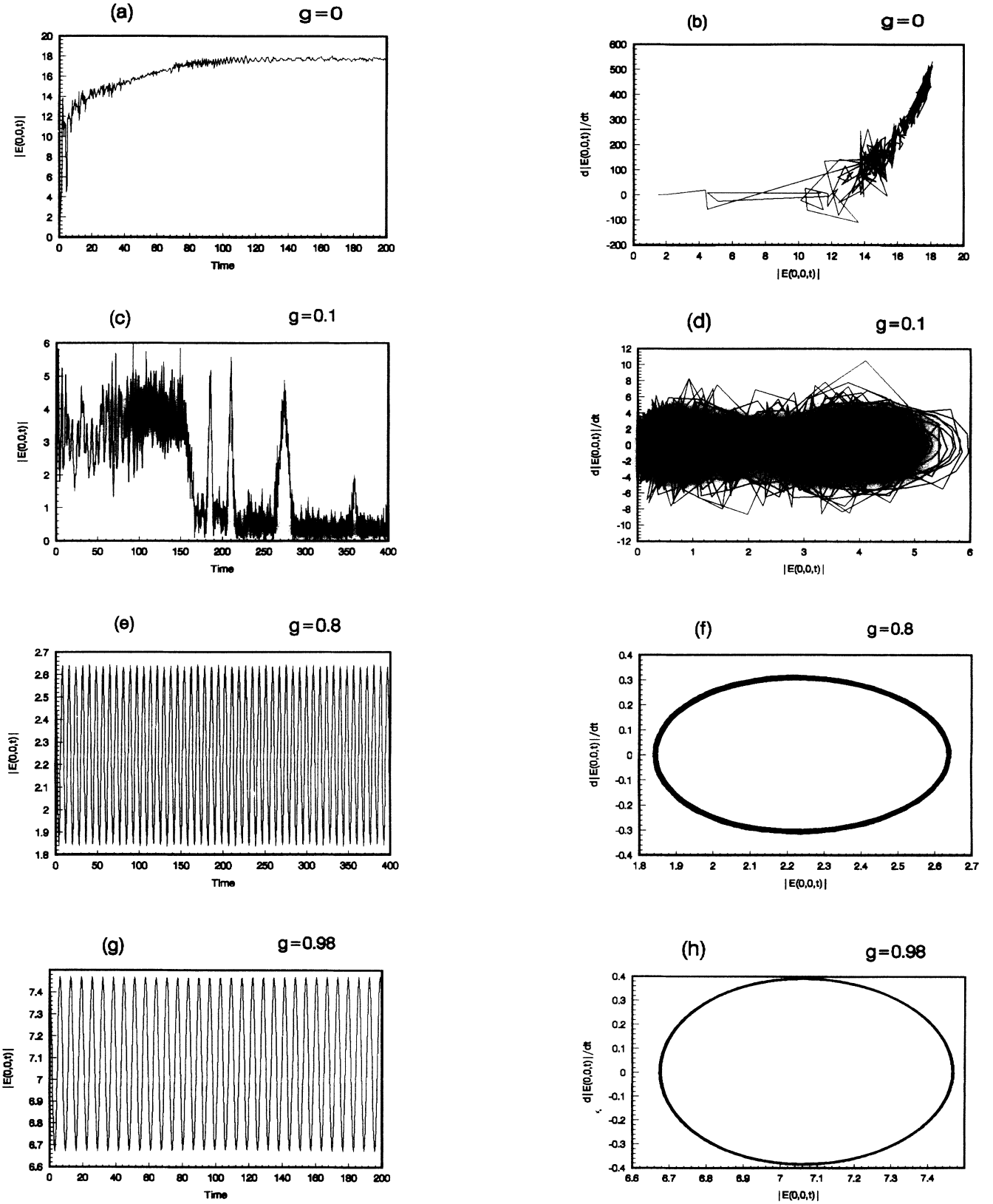

FIG. 12. Solutions of Eq. (5.1). (a), (c), (e), and (g) are the amplitude of fields, (b), (d), (f), and (h) the phase-space trajectory; (a) and (b) correspond to the singular solution with $g = 0$, (c) and (d) correspond to the chaotic solution with $g = 0.1$, and (e), (f) and (g), (h) correspond to the pseudorecurrent solutions with $g = 0.8$ and $g = 0.98$, respectively.

Taking into account these pictures for the case of pseudorecurrence, therefore, we can say that the symmetry of the solution is not basically broken down and the singular solution is completely prevented by the saturable nonlinearity.

D. Analyses of the energy spectrum

To illustrate clearly the mechanism that leads to the formation of these different complicated patterns, we also measure the evolution of the energy in the Fourier modes, and define

$$H = \sum_{K_{n,m}} |E(K_n, K_m, t)|^2, \tag{5.3}$$

where $K_{n,m} = \{K_n, K_m\}$ represents the nth Fourier mode in X space and the mth in Y space. The evolution of energy in Fourier modes, i.e., $H_{n,m} = |E_{K_n,K_m}|^2$, is shown in Figs. 17–19. Figure 17 corresponds to the case of $g = 0$, where we observe that the energy in the diagonal modes decays within a very short time and then stochas-

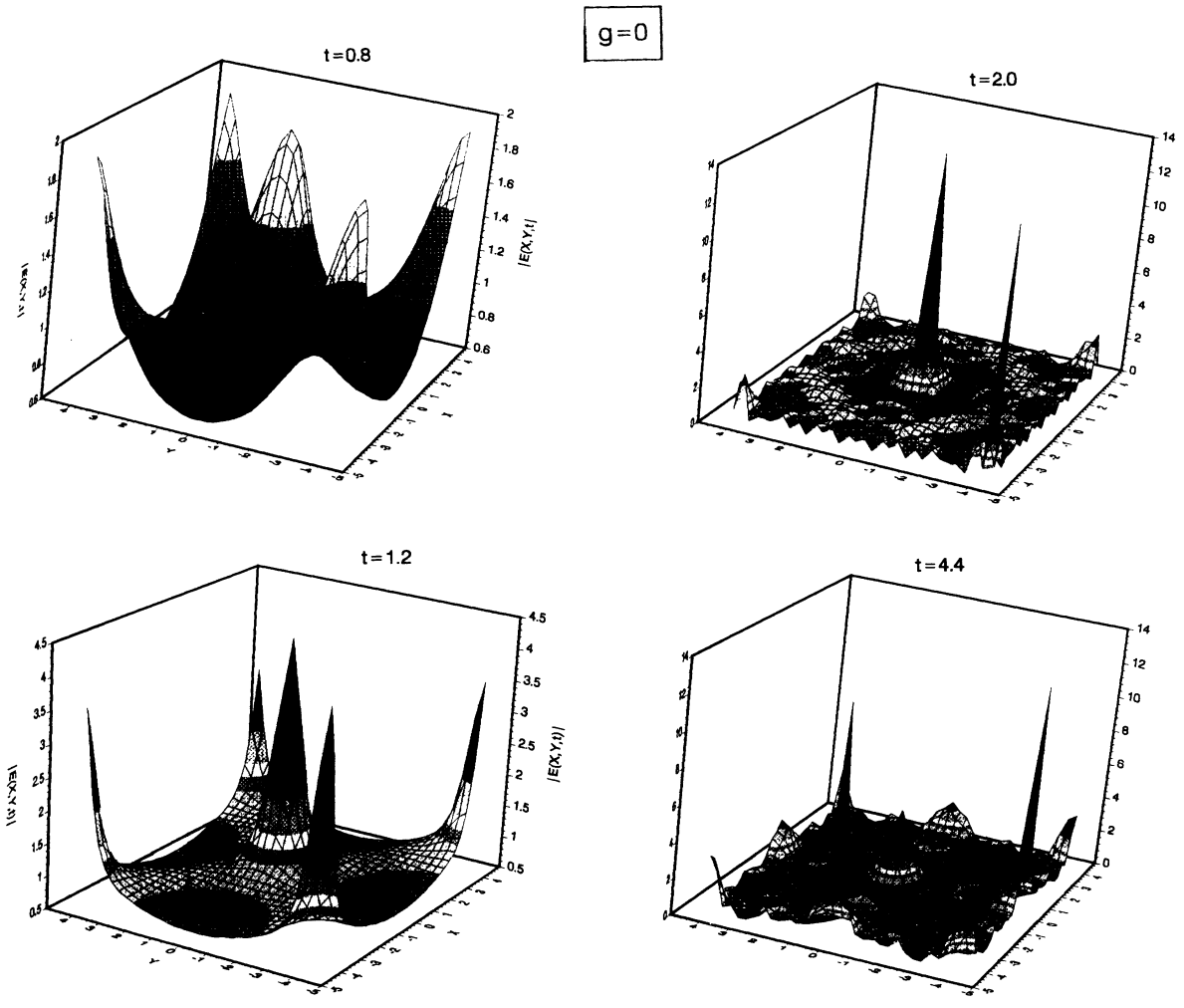

FIG. 13. The spatial patterns of the blowup processes with $g = 0$.

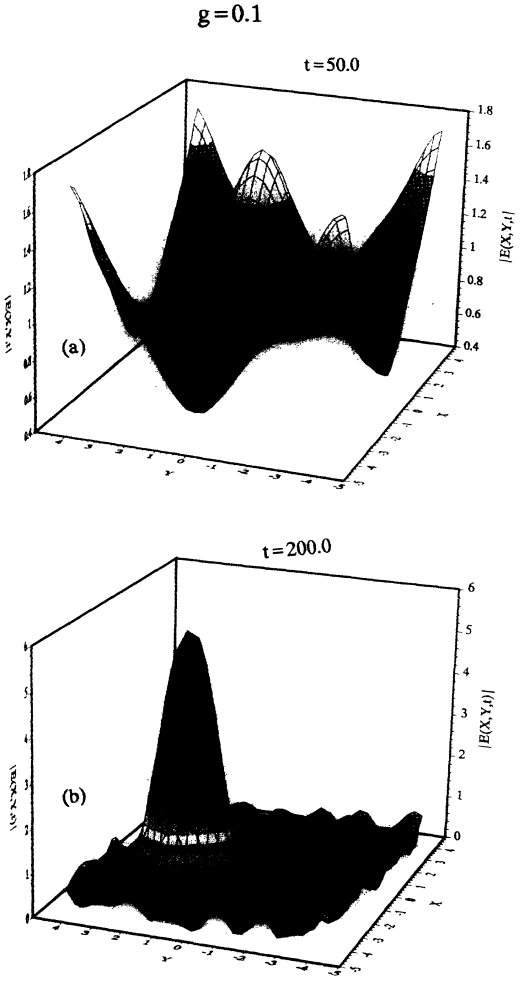

FIG. 14. The spatial patterns of spatiotemporal chaos with $g = 0.1$. (a) the symmetric structures, (b) the nonsymmetric structures.

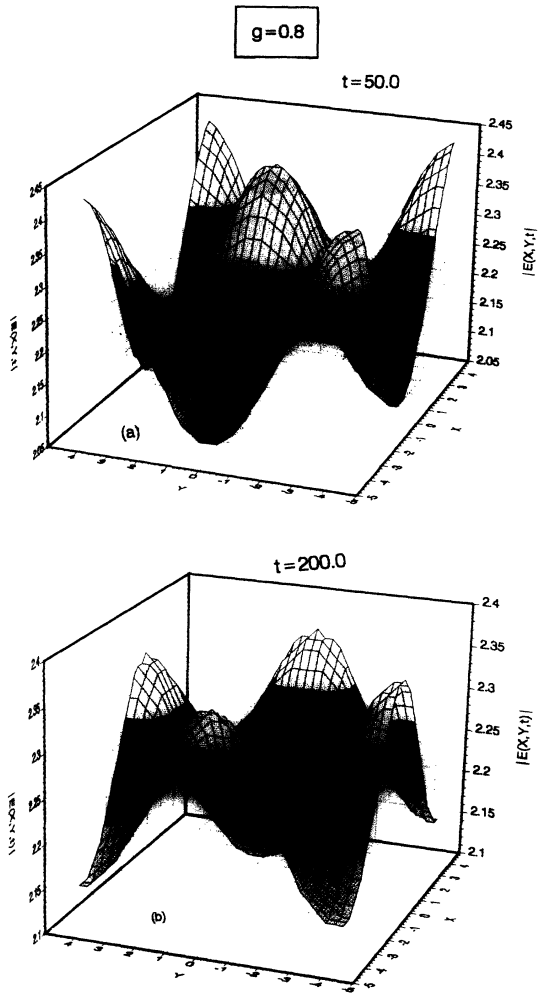

FIG. 15. The spatial patterns of the pseudorecurrent solution with $g = 0.8$.

tically oscillates. Also, the energy in the nondiagonal modes increases within a short time. In other words, time to reach the blowup may be associated with the evolution of the energy in the Fourier modes. When the blowup occurs, the energy in the main modes is decreased. In fact, the energy in these modes would determine the structures of the system. If the energy in the diagonal modes is very large, then the width of the wave packets would be large enough, which indicates that the blowup does not occur. With the development of time, the energy in the diagonal modes decreases and that in the nondiagonal modes increases. At this time, the energy in the system would be concentrated on some small spots, which shows that the singular solution occurs. Moreover, the nonsymmetric patterns may appear [see Fig. 13(c) and Fig. 13(d)] as soon as the energy in the nondiagonal modes is quite large.

It is noticed from Fig. 18 that an important phenomenon is exhibited. When $t < 60$, the energy in the diagonal modes experiences a stochastic oscillation. Simultaneously, their largest amplitude is near equal though the amplitude is actually stochastic. In particular, the energy in the nondiagonal modes equals zero for $t < 60$. When $t > 60$, the energy in the diagonal modes is decreased, and that in the nondiagonal modes is increased but still has the stochastic characteristic. In addition, we find that a large part of the energy lies in the main mode (K_{00}), where the initial energy is injected. According to these analyses, a clear conclusion is that the spatially nonsymmetric structures are mainly dependent on the energy in the nondiagonal modes. That is, the nonsymmetry should be associated with a stochastic partition of the energy in the Fourier modes, especially in the nondiagonal modes. Comparing Figs. 13 and 14 with Figs. 17 and 18, also, we conclude that the concentration of energy in the system depends on the distribution of the

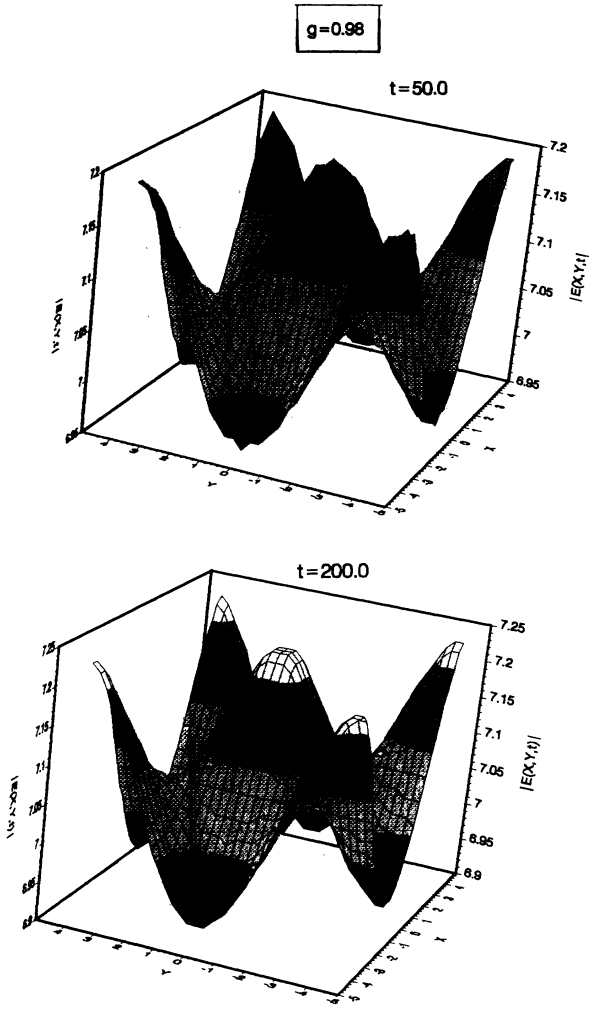

FIG. 16. The spatial patterns of the pseudorecurrent solution with $g = 0.98$.

energy in the Fourier modes. That is, the less energy is partitioned in the diagonal modes or the more in the nondiagonal modes, the higher the height of the spatial patterns is or the smaller the width.

Now, we discuss the spectrum evolution corresponding to the pseudorecurrent solution. From Fig. 19, we see that the energy in the main mode K_{00} compared with the other modes is very large and oscillates within a small regime. The evolution of the energy in the diagonal modes exhibits a periodiclike motion. In particular, the energy in mode K_{22} indicates the energy is not exactly FPU recurrent, but the partition of the energy in this mode is not irregular, which actually illustrates the pseudorecurrent feature. On the other hand, we find from the numerical experiments that the energy in the nondiagonal modes is nearly zero, which shows that the spatial structures developed by the modulational instability are symmetric, as seen in Fig. 15.

VI. SUMMARIES AND DISCUSSIONS

We have systematically described the spatiotemporal characteristics of a series of generalized NSE's in one- and two-dimensional space. Our investigations show that a high order Hamiltonian perturbation can lead to the destruction of the coherent structures and the formation of spatiotemporally complicated patterns. The route from coherent patterns to complicated ones is quasiperiodic. For two-dimensional problems, our numerical experiments illustrate that the singular solution, spatiotemporal chaos, and pseudorecurrence can appear for the same NSE with the increase of the saturable nonlinear effects, where the spatial patterns and the energy partition of the system in the Fourier modes exhibit completely different dynamic behaviors. We emphasize in particular that the symmetric destruction of the spatial patterns is associated with the energy in the nondiagonal modes. These results should be of significance in the study of pattern dynamics in plasma waves and other nonlinear waves.

As far as various branches of physics are concerned, the presence of the stochastic wave fields depends on the evolution processes of systems. In other words, the lowest order nonlinear term $|E|^2E$ is the predominant nonlinear mechanism in the evolving initial stages. Some important phenomena, such as coherent structures and Langmuir wave collapse, etc., can be reasonably explained by making use of the cubic NSE. In the strongly nonlinear stages, other physical effects could play an important role. For example, the effects of Landau damping of the high frequency waves become quite significant in plasma turbulence. The energy dissipation should be considered [38,39]. On the other hand, nonlinear interactions, such as the fourth field interaction and other nonlinear saturable mechanisms, should be involved in the processes of plasma instabilities. These nonlinear saturable effects make rich dynamic behaviors occur. In a sense, these complicated dynamic phenomena would probably be the characteristic of wave propagation.

We should mention that our results are also important in laser fusion studies. Considering the process of ponderomotive filamentation, under the static approximation, one studies the characteristics of ponderomotive filamentation in terms of the NSE's (1.6)–(1.9) [25–28,37] when the time variable t is replaced by the spatial variable Z. It is shown that the focusing becomes a periodic oscillation, rather than a catastrophic process due to the saturable effects. In the previous work, it was illustrated that there exists competition between SBS and filamentation instability [25,26]. Taking into account filamentation produced by perturbations or nonuniformities in light that cause (or are caused by) local changes in the dielectric constant, index of refraction, or the medium, we easily understand that these inhomogeneities may be enlarged due to mode-mode interactions, where the transverse instability as described in this work or the self-modulation as discussed by Max *et al.* [40] can broaden the frequency spectrum of the incident laser. For these

instabilities, as a matter of fact, there is no reason to separate them in the nonlinear regime. They can coexist and affect each other. Of course, SBS is related to the resonant interaction of a three-wave coupling, whereas self-focusing and filamentation instabilities involve nonresonant ion density disturbances. As far as the stochastic instabilities are concerned, the mode-mode resonant interaction [41] may also drive the chaotic propagation of light. The current investigations show that an initial homogeneous beam may develop into incoherent light, where the symmetry of the laser could be broken down and the center of the beams would be shifted off axis due to the influence of the ponderomotive force. Of course, the recent modulation should be the spatial modulation in the transverse direction, because the starting equations (1.6)–(1.9) only allow for transverse inhomogeneities when the time variable t is replaced by the axial variable Z.

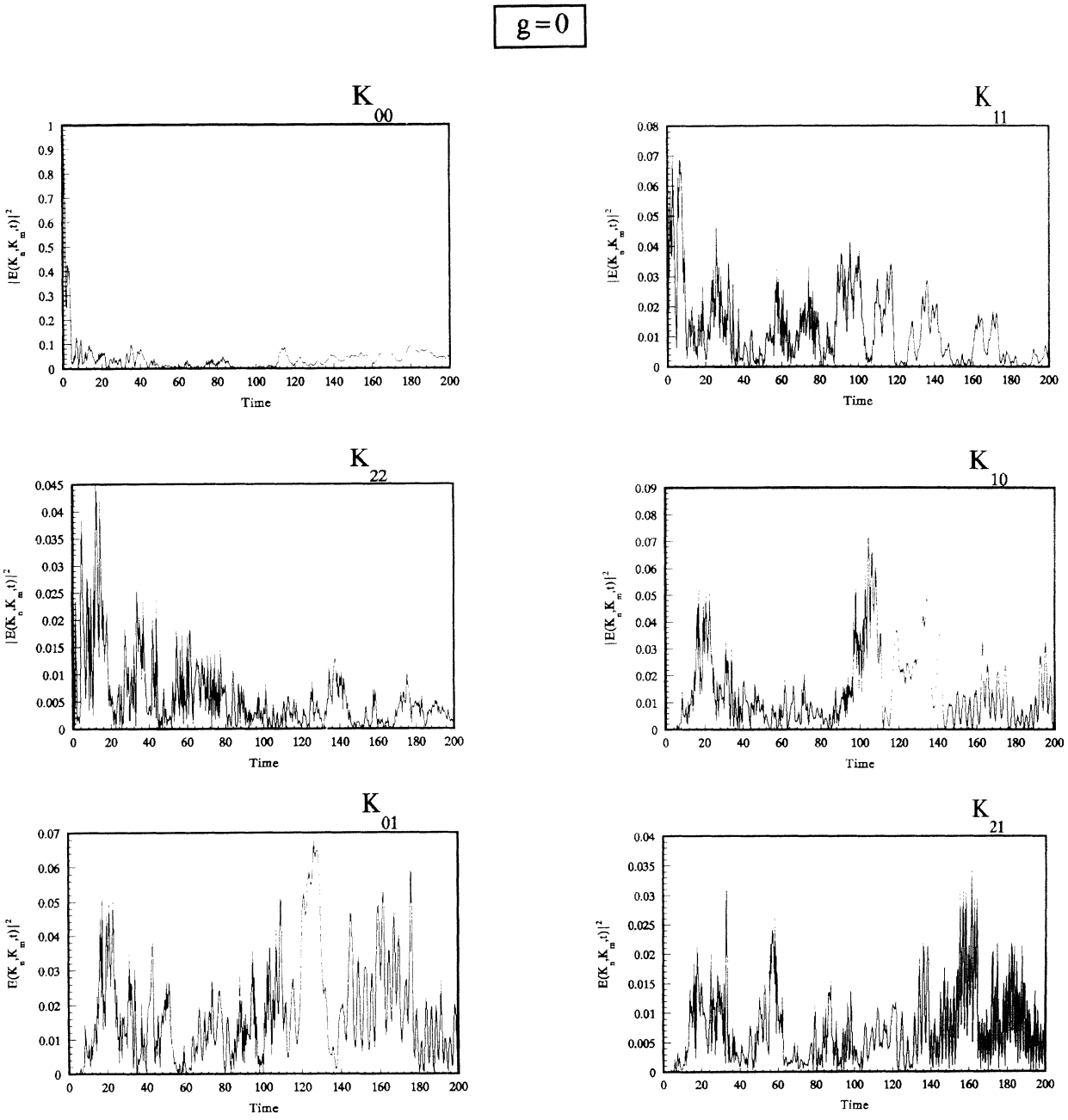

FIG. 17. The evolution of the energy in the Fourier modes with $g = 0$.

Finally, we point out that our work only deals with the initial homogeneous state. It is shown that the presence of the HMO crossings is a potential source of stochastic behavior. We expect that more important theoretical work on HMO chaos in the continuum Hamiltonian system can be furthered in future study. We also note that it is an interesting and important piece of research for us to consider the initial inhomogeneous state, which could be more difficult for theoretical analysis as in this work. We think that the key problem should still be the constitution of a suitable phase space for these continuum Hamiltonian systems so that one can readily describe their dynamic characteristics in terms of integrable and nonintegrable equations.

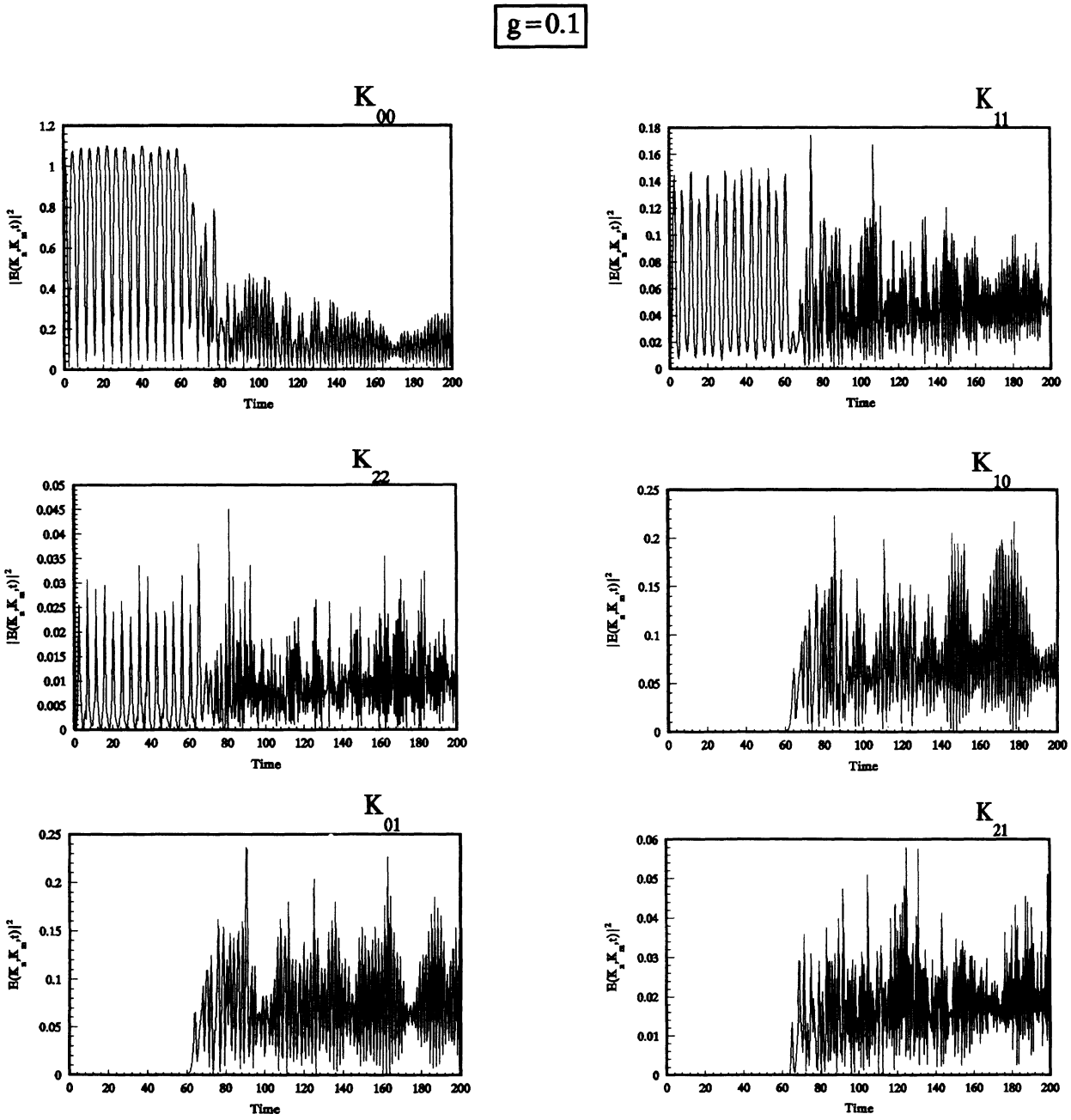

FIG. 18. The evolution of the energy in the Fourier modes with $g = 0.1$.

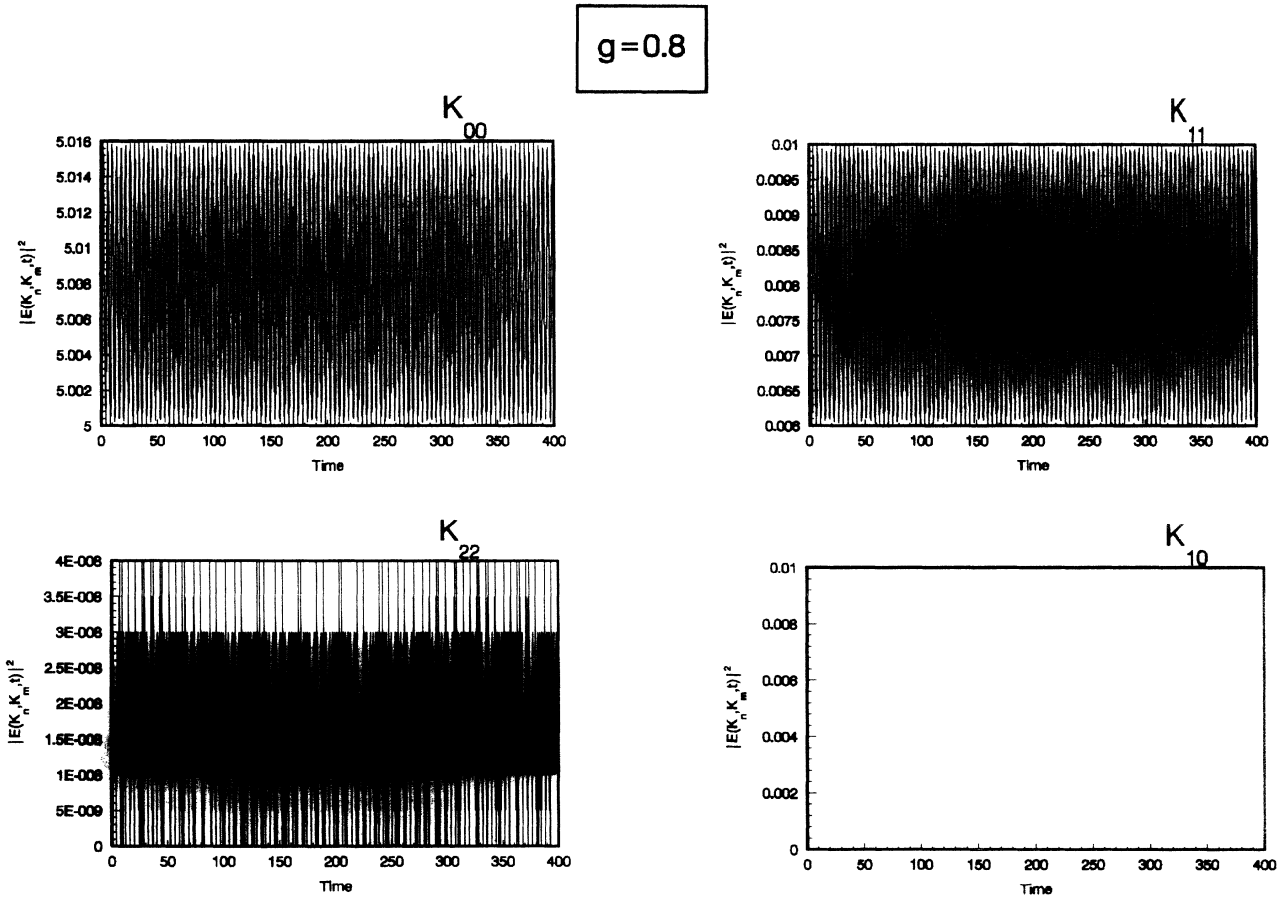

FIG. 19. The evolution of the energy in the Fourier modes with $g = 0.8$.

ACKNOWLEDGMENTS

One of us (C. T. Zhou) wishes to acknowledge useful discussions on filamentation instability in the NSE with Professor T. W. Johnston, and is grateful to Professor S. G. Chen, Professor J. L. Zhang, and Professor L. J. Shen for helping in theoretical analyses and numerical discussions. This work is supported by the CAEP foundation, Grant No. HD9317 (C.T.Z), and in part by the Natural Science Foundation of China (NSFC) and Nonlinear NSFC.

[1] P. L. Kelley, Phys. Rev. Lett. **15**, 1005 (1965).
[2] M. J. Alblowitz and H. Segur, J. Fluid Mech. **93**, 691 (179).
[3] T. Taniuti and H. Washimi, Phys. Rev. Lett. **21**, 209 (1968).
[4] V. E. Zakharov and A. B. Shabat, Zh. Eksp. Teor. Fiz. **61**, 118 (1972) [Sov. Phys. JETP. **34**, 62 (1972)].
[5] V. E. Zakharov, S. V. Manakov, S. Novikov, and L. P. Pitayevsky, *Introduction to the Theory of Solitons* (Plenum, New York, 1983).
[6] J. J. Rasmussen and K. Rypdal, Phys. Scr. **33**, 481 (1986).
[7] V. G. Makhankov, *Soliton Phenomenology* (Reidel, Dordrecht, 1989).
[8] M. V. Goldman, Rev. Mod. Phys. **54**, 709 (1984).
[9] B. M. Lake, H. C. Rungaldier, and W. E. Ferguson, J. Fluid Mech. **83**, 49 (1977).
[10] H. C. Yuen, B. M. Lake, and W. E. Ferguson *The Significance of Nonlinearity in the Natural Science* (Plenum, New York, 1977).
[11] H. C. Yuen and W. E. Ferguson, Jr., Phys. Fluids **21**, 1275 (1978).
[12] M. Stiassnie and U. I. Kroszynski, J. Fluid Mech. **116**, 207 (1982).
[13] X. T. He, Acta Phys. Sin. **30**, 1415 (1981).
[14] R. V. Djolos, V. G. Kartavenko, and V. G. Permyakov, Yad. Fiz. **34**, 1444 (1981) [Sov. J. Nucl. Phys. **34**, 800 (1981)].
[15] K. I. Pushkarov, D. I. Pusharov, and I. V. Tomov, Opt. Quantum Electron. **11**, 471 (1979).

[16] S. Cowan, R. H. Enns, S. S. Rangnekar, and S. S. Sanghera, Can. J. Phys. **64**, 311 (1986).
[17] L. Gagnon and P. Winternitz, J. Phys. A **21**, 1489 (1988).
[18] L. Gagnon and P. Winternitz, J. Phys. A **22**, 469 (1989).
[19] C. T. Zhou, X. T. He, and S. G. Chen, Phys. Rev. A **46**, 2277 (1992).
[20] A. Cloot, B. M. Herbst, and J. A. C. Weideman, J. Comput. Phys. **86**, 127 (1990).
[21] L. Gagnon and P. Winternitz, Phys. Rev. A **39**, 296 (1989).
[22] N. N. Akhemediev, D. R. Heatley, G. I. Stegement, and E. M. Wight, Phys. Rev. Lett. **65**, 1423 (1990).
[23] (a) D. W. Mclaughin, G. Papanicolaou, C. Sulem, and P. L. Sulem, Phys. Rev. A **34**, 1200 (1986); (b) B. J. Lemsurier, G. Papanicolaou, C. Sulem, and P. L. Sulem, Physica D **31**, 78 (1988).
[24] P. K. Shukla, in *Solitons in Plasma Physics in Nonlinear Waves*, edited by L. Debnath (Cambridge University Press, London, 1983), Chap. 11.
[25] C. E. Max, Phys. Fluids **19**, 74 (1976).
[26] J. F. Lam, B. Lippmann, and F. Tappert, Phys. Fluids **20**, 1176 (1977).
[27] P. Kaw, G. Schmidt, and T. Wilcox, Phys. Fluids **16**, 1522 (1973).
[28] C. T. Zhou and X. T. He (unpublished).
[29] D. R. Nicholson, *Introduction to Plasma Theory* (Wiley, New York, 1983).
[30] M. S. Cramer and L. T. Watson, Phys. Fluids **27**, 821 (1990).
[31] J. Guckenheimer and P. Holms, *Nonlinear Oscillations, Dynamical Systems, and Bifurcations of Vector Fields* (Springer-Verlag, New York, 1983).
[32] (a) T. R. Taka and M. A. Ablowitz, J. Comput. Phys. **55**, 203 (1984); (b) M. D. Feit *et al.*, J. Opt. Soc. Am. B **5**, 639 (1988).
[33] T. B. Benjamin and J. E. Feir, J. Fluid Mech. **27**, 417 (1967).
[34] A. J. Lichtenberg and M. A. Lieberman, *Regular and Stochastic Motion* (Springer-Verlag, Berlin, 1984).
[35] C. T. Zhou and X. T. He, Phys. Rev. E **49**, 4417 (1994).
[36] C. T. Zhou, Ph.D thesis, Institute of Applied Physics and Computational Mathematics, Beijing, 1992.
[37] T. W. Johnston (unpublished).
[38] H. T. Moon, Phys. Rev. Lett. **64**, 412 (1990); see also the references therein.
[39] K. Nozaki and N. Bekki, (a) Phys. Rev. Lett. **50**, 1226 (1983); (b) Phys. Lett. **102A**, 383 (1984).
[40] C. E. Max, J. Arons, and A. B. Langdon, Phys. Rev. Lett. **33**, 209 (1974).
[41] R. Z. Segdeev, D. A. Usikov, and G. M. Zaslavsky, *Nonlinear Physics From the Pendulum to Turbulence and Chaos* (Harwood Academic, Chur, Switzerland, 1988).

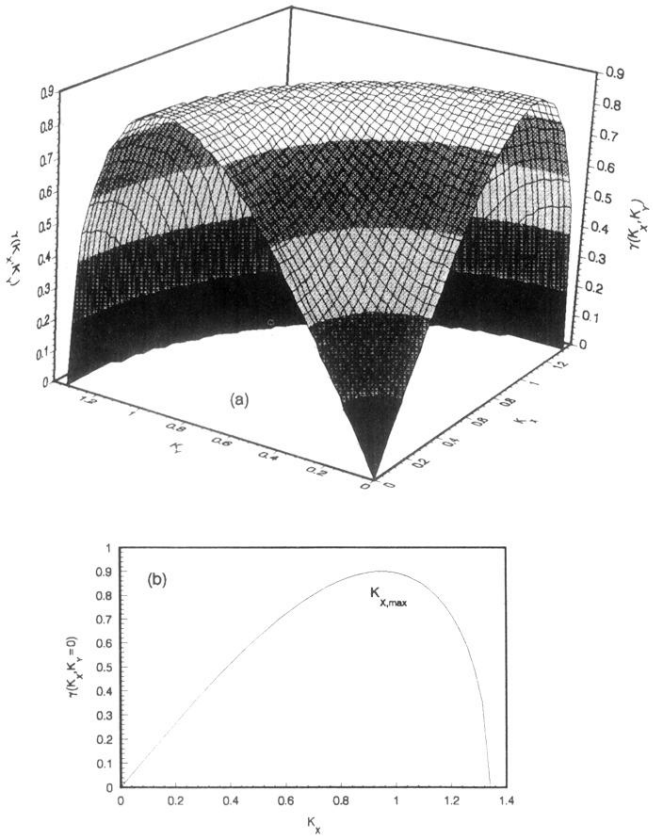

FIG. 10. (a) The linear growth rate vs K_X and K_Y. (b) The growth rate vs K_X with $K_Y = 0$.

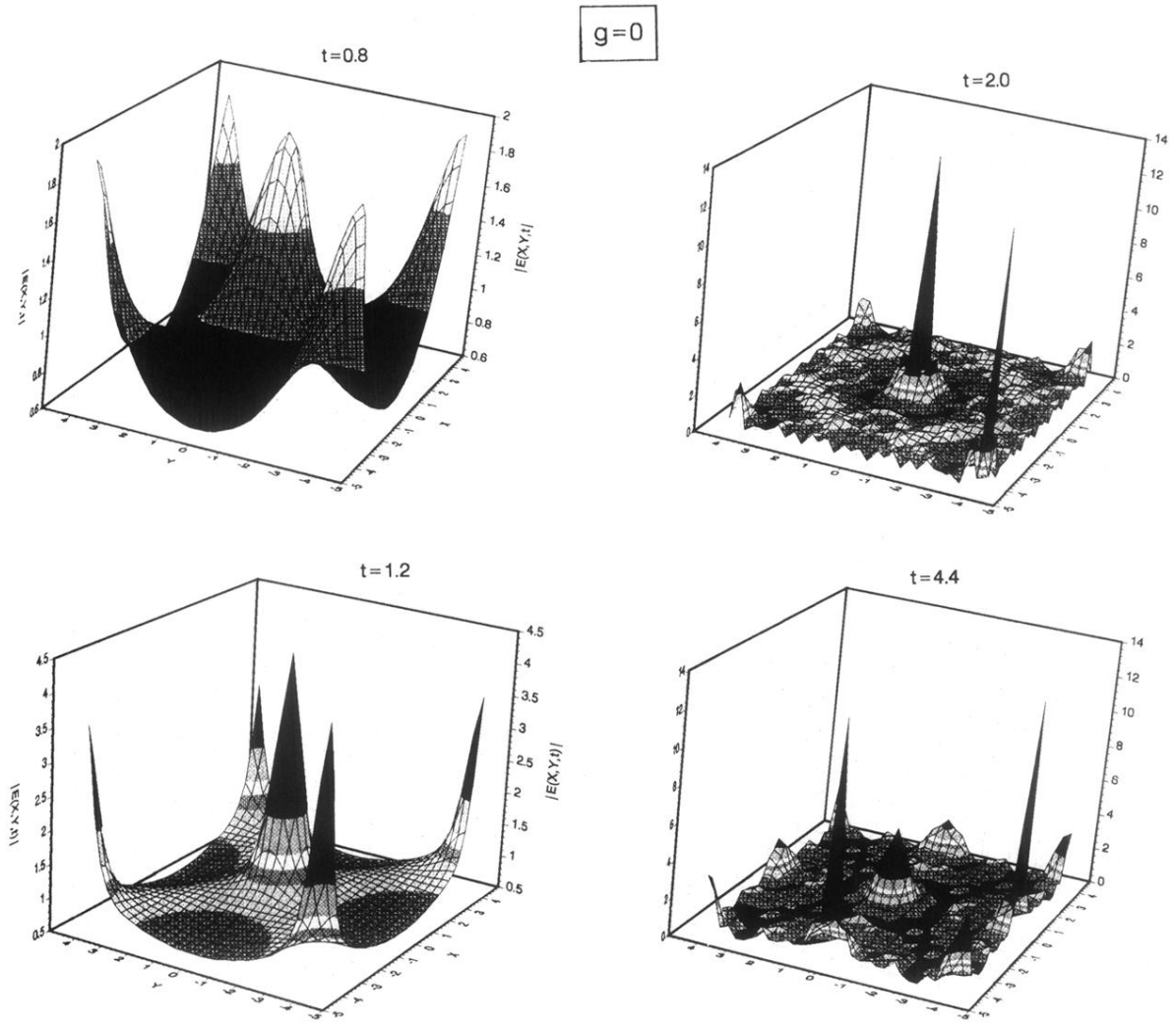

FIG. 13. The spatial patterns of the blowup processes with $g = 0$.

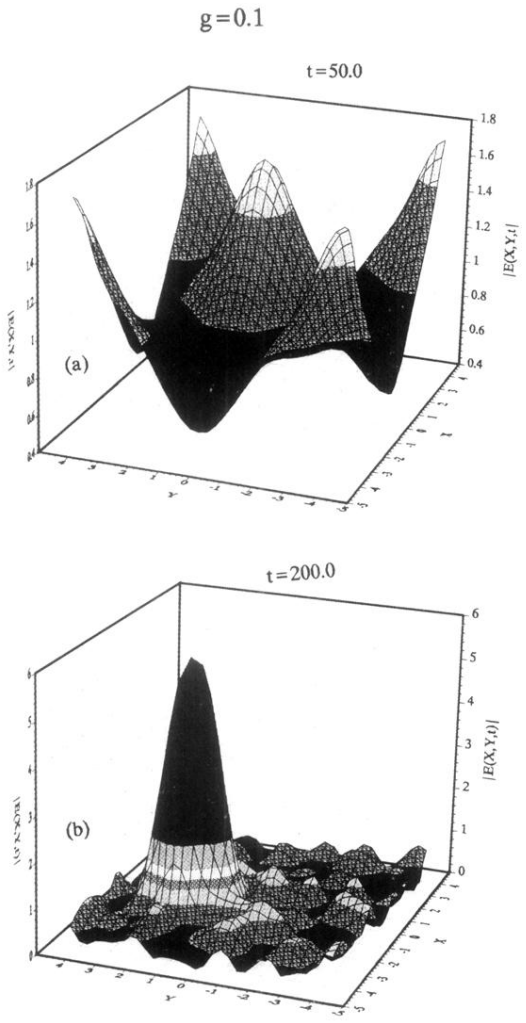

FIG. 14. The spatial patterns of spatiotemporal chaos with $g = 0.1$. (a) the symmetric structures, (b) the nonsymmetric structures.

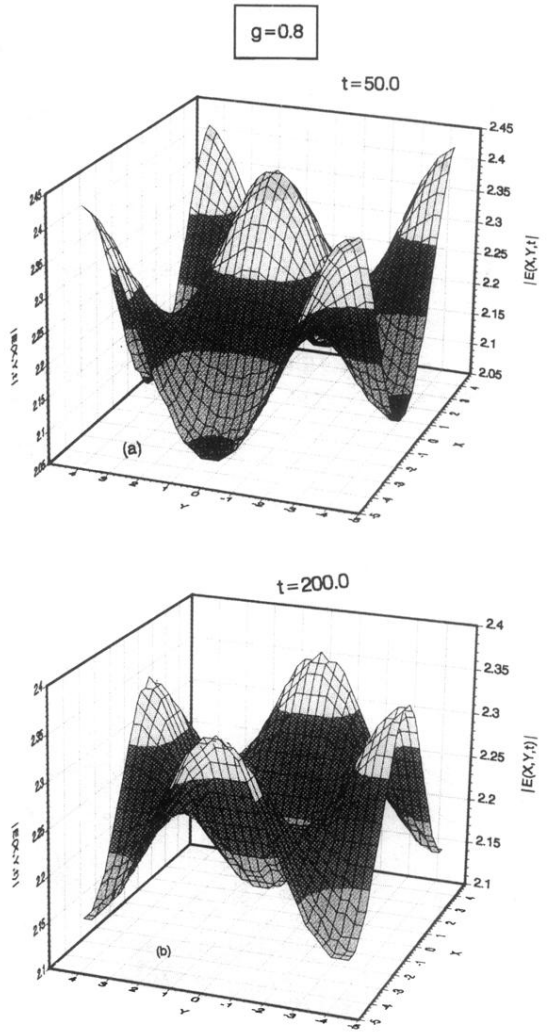

FIG. 15. The spatial patterns of the pseudorecurrent solution with $g = 0.8$.

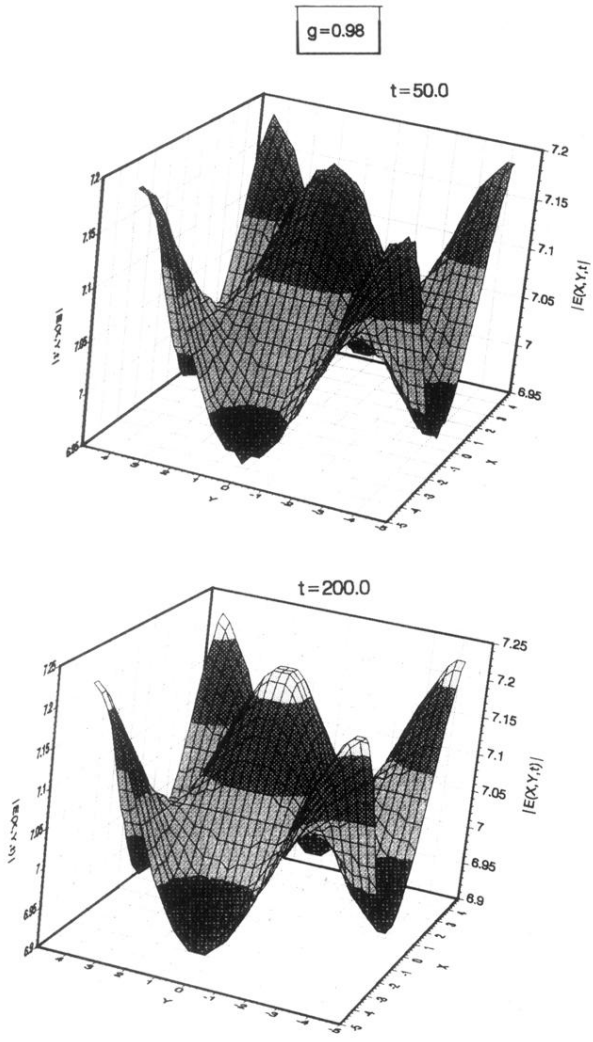

FIG. 16. The spatial patterns of the pseudorecurrent solution with $g = 0.98$.

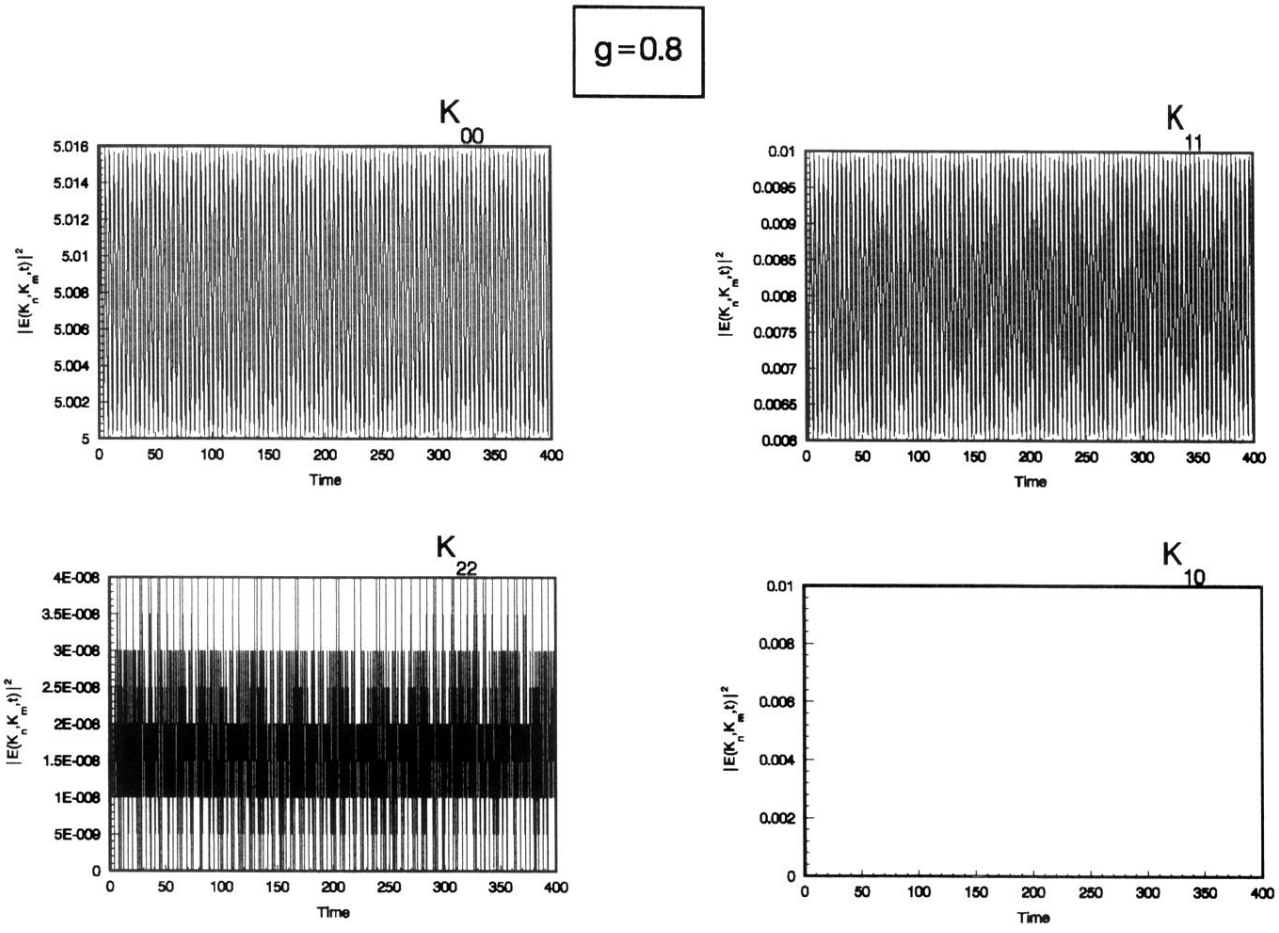

FIG. 19. The evolution of the energy in the Fourier modes with $g = 0.8$.

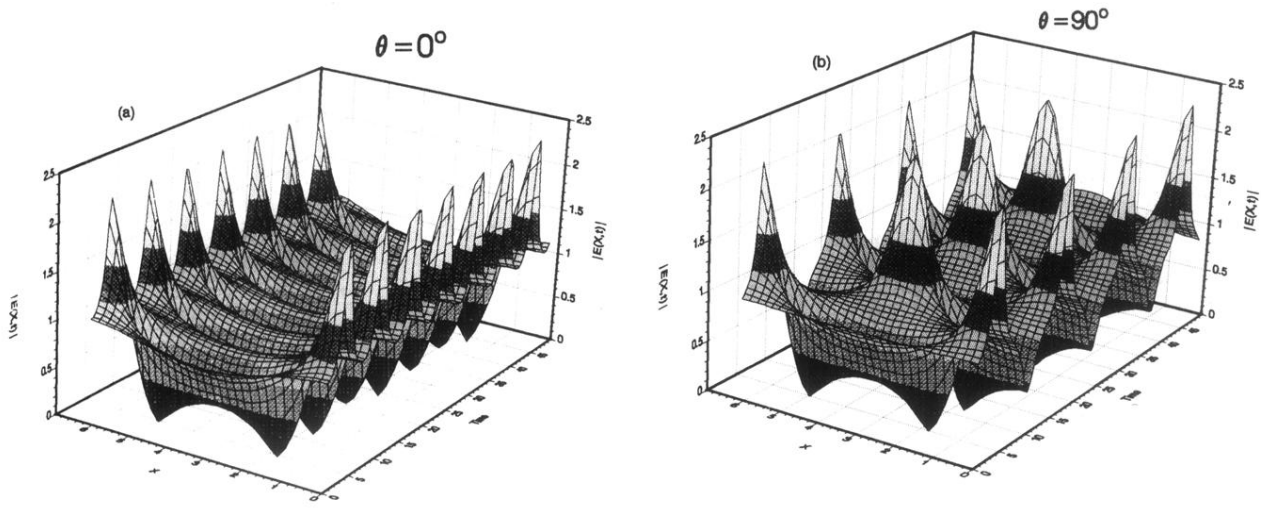

FIG. 4. The coherent structures of the one-dimensionally cubic NSE; (a) and (b) correspond to $\theta = 0°$ and $90°$, respectively.

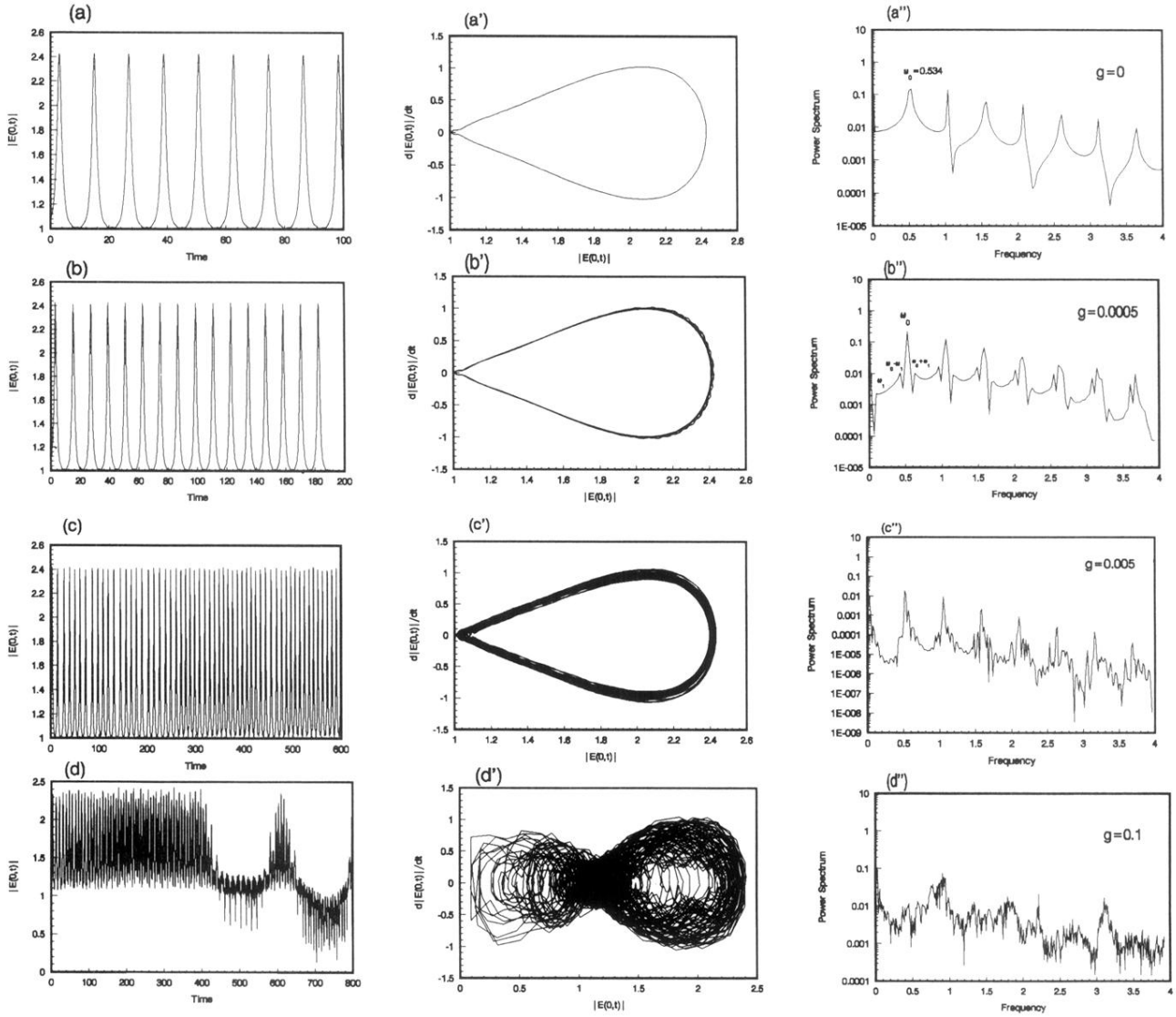

FIG. 7. The solutions of Eq. (4.4) with $\epsilon = 0.1$ and $\theta = \frac{1.0005\pi}{4}$, where a fixed position ($X = 0$) is traced. (a), (b), (c), and (d) correspond to the temporal evolution of amplitude for fields; (a′), (b′), (c′), and (d′) are the structures of phase space, noting that (d′) indicates the irregular homoclinic orbit crossings; (a″), (b″), (c″), and (d″) represent the power spectra corresponding to (a), (b), (c), and (d), respectively. In particular, (b′) exhibits the quasiperiodic spectrum.

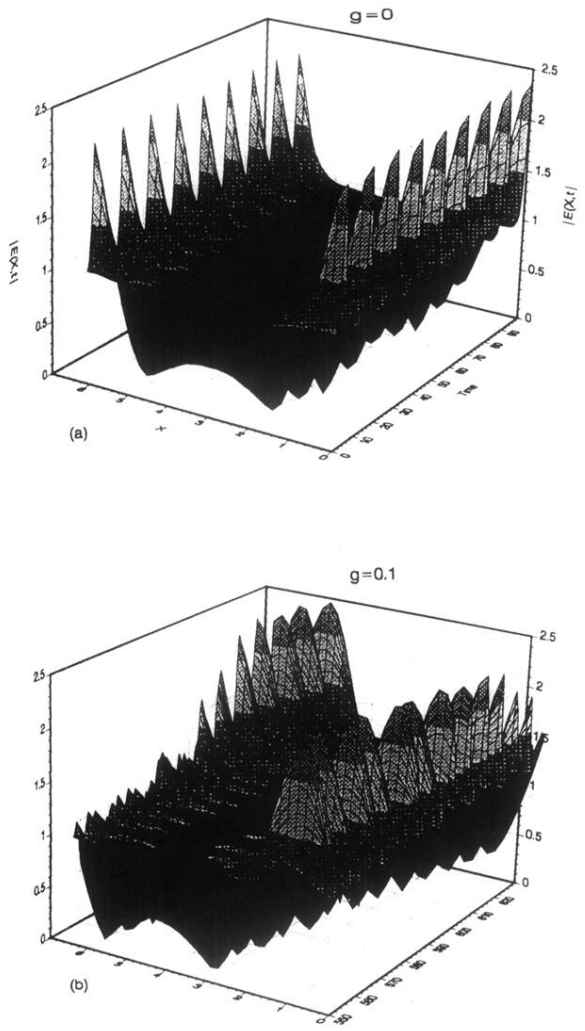

FIG. 8. The spatiotemporal patterns for the saturable NSE (4.4) with $\epsilon = 0.1$ and $\theta = \frac{1.0005\pi}{4}$, but the value g changed. (a) Coherent patterns with $g = 0$; (b) spatiotemporally complicated patterns with $g = 0.1$.